Impact of SST on heavy rainfall events on eastern Adriatic during SOP1 of HyMeX

Stjepan Ivatek-Šahdan[a], Antonio Stanešić[a], Martina Tudor[a], Iris Odak Plenković[a], Ivica Janeković[b,c]

[a] *Croatian Meteorological and Hydrological Service, Grič3, Zagreb, Croatia*
[b] *Rudjer Bošković Institute, Bijenička 54, Zagreb, Croatia*
[c] *The University of Western Australia, School of Civil, Environmental and Mining Engineering & UWA Oceans Institute, Crawley, WA 6009, Australia*

Abstract

The season of late summer and autumn is favourable for intensive precipitation events (IPE) in the central Mediterranean. During that period the sea surface is warm and contributes to warming and moistening of the lowest portion of the atmosphere, particularly the planetary boundary layer (PBL). Adriatic sea is surrounded by mountains and the area often receives substantial amounts of precipitation in short time (24 hours). IPEs are a consequence of convection triggered by topography acting on the southerly flow that has brought the unstable air to the coastline. Improvement in prediction of high impact weather events is one of the aims of The Hydrological cycle in the Mediterranean eXperiment (HyMeX). This study examines how precipitation patterns change in response to different SST forcings. We focus on the IPEs that occured on the eastern Adriatic coast during the first HyMeX Special observing period (SOP1, 6 September to 5 November 2012). The operational forecast model ALADIN uses the same SST as the global meteorological model (ARPEGE from Meteo France), as well as the forecast lateral boundary conditions (LBCs). First we assess the SST used by the operatonal atmospheric model ALADIN and compare it to the in situ measurements, ROMS ocean model, OSTIA and MUR analyses. Results of this assessment show that SST in the eastern Adriatic was overestimated by up to 10 K during HyMeX SOP1 period. Then we examine the sensitivity of 8 km and 2 km resolution forecasts of IPEs to the changes in the SST. Forecast runs in both resolutions are performed for the whole SOP1 using different SST fields prescribed at initial time and kept constant during the

model forecast. The results show that the impact of introducing improved SST in the analysis on the precipitation forecast varies for different cases. There is generally a larger sensitivity to the SST in high resolution than in the lower one, although the forecast period of the latter is longer.

Keywords: intensive precipitation events, sea surface temperature, numerical weather prediction

---

1. Introduction

Intensive precipitation events (IPEs) of more than 100 mm in 24 hours are regularly recorded over the region of central Mediterranean. These events can lead to flash floods and cause substantial damages and occasionally human casualties (Silvestro et al., 2012; Rebora et al., 2013; Ivančan-Picek et al., 2014). The most severe IPEs are often associated to synoptic situations with blocking when weather systems are more stationary in space and time (Doswell et al., 1996; Homar et al., 2002). The mountains surrounding the Adriatic can trigger or enhance stationary mesoscale convective system (MCS) associated to southerly flow advecting moist air from the Mediterranean/Adriatic Sea (Ivančan-Picek et al., 2014; Mastrangelo et al., 2011). The conditional convective instability is increased by the moisture and heat released by the warm sea in late summer and autumn.

Small et al (2008) give an overview of the air-sea interaction over fronts and eddies and find that surface stress is positively correlated with SST. The atmospheric boundary layer over ocean responds to the surface heat fluxes by forming an internal boundary layer, differences in turbulent transfer of momentum, hydrostatic pressure anomalies and change in boundary layer height.

Mesoscale SST data improve the representation of heat fluxes at the interface of atmosphere and sea (Weill et al., 2003). Several studies have examined the role of SST in the rainfall events over the central Mediterranean (Davolio et al., 2016; Stocchi and Davolio, 2016) and more have focused on the western Mediterranean (Romero et al., 1997; Pastor et al., 2001; Lebeaupin et al., 2006) using numerical weather prediction models. Generally, evaporation and convection are more intensive with higher SST, but shifting SST by a fixed amount can also yield a shift in the position of the maximum rainfall (Stocchi and Davolio, 2016). In a recent study of the role of the SST in IPEs in the Ligurian sea, Cassola at al. (2016) analyze numerical simulations of

MCSs using coarse and high resolution SST data and find that the effect of the SST on the location of the peak precipitation intensity is rather limited due to the prevailing influence of topography.

The fluxes of heat and moisture at the air-sea interface contribute to warming and moistening of the PBL. That destabilizes the air mass and can trigger convection. The statistical relationship of the maximum intensity in the tropical cyclones on SST exists in data but it is not reproduced by the climate models (Strazzo et al., 2016) due to low resolution or too strong wind shear in the models. Colder SST can supress convection over the sea, but it does not vanish completely from the model forecast. These effects vary from case to case and can have negligible impact in the first 12 hours (Romero et al., 1997). Sensitivity tests have been performed using hydrostatic models with parametrized convection and high resolution non-hydrostatic models (Pastor et al., 2001; Lebeaupin et al., 2006) where convection is considered explicitly resolved. The precipitation forecast can be significantly improved when SST field is based on measurements (Pastor et al., 2001). Also, a direct relation of the simulated precipitation to the areally averaged SST has been suggested (Pastor et al., 2001).

From 6 September to 5 November 2012, the first Special Observing Period (SOP1) of the HYdrological cycle in the Mediterranean eXperiment (HyMeX) programme is performed (Drobinski et al., 2014) with an aim to improve understanding and forecast of intensive rainfall in the Mediterranean region (Ducrocq et al., 2014). Since one of the aims of HyMeX is to improve the ability of numerical weather prediction (NWP) models in forecasting the location and intensity of heavy precipitation events in the Mediterranean, we focus on the SOP1 to investigate the influence of SST on the forecast of IPE.

Heavy precipitation events often affects the eastern Adriatic coastline leading to flash floods and extensive damages (Mazzocco Drvar et al., 2012; Ivančan-Picek et al., 2014). The local mountains, Dinaric Alps, are arranged parallel to the coastline with peaks of more than 1.5 km high, less than 10 km from the shore (Figure 1). The Alps on the north have a profound influence on the atmospheric motions in the area by orographic cyclogenesis while local mountains (Dinaric Alps) provide orographic uplift and trigger heavy precipitation. The Mediterranean and particularly the Adriatic Sea are sources of moisture and heat for the air mass that is subsequently transported towards the mountains.

Higher SSTs are usually associated with increased convection and more

intensive precipitation (Trenberth and Shea, 2005) in high latitudes and in the tropics where intensive precipitation can be a consequence of sharp SST gradients (Toy and Johnson, 2014). However, Trenberth and Shea (2005) also show negative corelation between temperature and precipitation for midlatitudes and Mediterranean in the summer season.

Most of operational NWP models keep the initial values of SST throughout the model forecast. This is not realistic in situations when the air-sea fluxes are intensive over small, enclosed and shallow basins, such as the Adriatic sea (Davolio et al., 2015). SST initialization represents a critical issue for an accurate description of surface fluxes at least for the severe events of intensive precipitation. An accurate description of surface fluxes (above sea surface) depends on the SST used in initial conditions (Davolio et al., 2015) as it does not change during the model forecast (Stocchi and Davolio, 2016).

The low level flow over the sea surface is influenced by the SST that modifies its thermodynamic profile. When this flow approaches a mountain that is preceeded by a valley the position of precipitation maximum depends on several factors. As distinguished by Davolio et al. (2016), depending on the thermodynamic profile of the atmospheric flow, convection can be triggered upstream of the mountain when the flow is forced to rise over a pre-existing cold air pool (over the valley) before the mountain and the heavy rain is localized over the plain. On the other hand, if this convection does not develop over the valley (due to absence of the cold air pool or thermodynamic profile of the impinging air that supports flow over conditions), then heavy rain affects the mountains.

Sudden and intensive cold air outbreaks and cold and dry wind such as bura (Grisogono and Belušić, 2009) can reduce SST by several degrees on a time scale of less than one day. Allowing SST to change during the forecast run could improve the forecast, and forecast quality is rather important in such severe weather events. We do not perform such a test in this paper, but identify cases and areas where it could be important.

The purpose of this study is to evaluate SST used in the operational forecast and to examine the sensitivity of 8 km and 2 km resolution forecasts of IPEs on eastern Adriatic coast that occured during HyMeX SOP1 to the SST. Here we show that the SST used in operational NWP model was overestimated for up to 10 K in Velebit Channel (VC) and Rijeka Bay during HyMeX SOP1. Consequently, operational high resolution forecast substantially overestimated the precipitation intensity over Velebit mountain. Also, reducing SST enhances precipitation for Rijeka area where maximum precip-

itation was indeed recorded.

All experiments are performed using ALADIN (Aire Limitée Adaptation Dynamique développement InterNational, ALADIN International Team (1997)) limited area model (LAM). The reference simulations for the whole period are operational forecasts (Tudor et al., 2013) that use SST from the initial file of the global model ARPEGE (Action de Recherche Petite Echelle Grande Echelle), that was operational at the time (Météo France, 2012). The operational forecasts do simulate IPEs (Ivančan-Picek et al., 2016), but the 8 km resolution forecast puts the peak intensity of precipitation over mountains inland from Rijeka. On the other hand, the operational high resolution run does forecast IPE for Rijeka, but tends to overestimate precipitation in certain areas, such as the Velebit mountain, particularly its southern part. First, several experiments are performed where the SST in the analysis is shifted by a fixed value. Then another set of experiments is performed in which the SST in the analysis is replaced by SST from OSTIA (UK Met Office, 2005) and MUR (JPL MUR MEaSUREs Project, 2015) analyses and then from the ROMS (Janeković et al., 2014) ocean model. The sensitivity of simulated precipitation to SST is then evaluated by comparing the results from experiments that use different SST fields to the reference operational forecast.

The paper is organized as follows. The model simulations and characteristics of different SST fields used in experiments are described in Section 2. Section 3 describes the results of simulations using different SST fields. The discussion and summary are in Section 4.

2. Methodology

The main objective of this study is to examine how precipitation patterns change in response to different SST forcings for IPEs. Our model simulations cover the entire HyMeX SOP1 period: from 6th September to 5th November 2012 when 8 events with precipitation exceeding 100 mm in 24 hours over eastern Adriatic occured (Ivančan-Picek et al., 2016). Operationally, at the time of HyMeX SOP1, SST was taken from the operational forecast of the global model ARPEGE, that was also used for the forecast lateral boundary conditions. The effect of SST on precipitation forecast was first analysed by increasing or decreasing the SST by a fixed amount. The subsequent set of experiments used SST from OSTIA and MUR analyses and ROMS ocean model. We focused on IPEs that occured during HyMeX SOP1, which took

place in late summer and autumn 2012, and provided a number of IPEs on eastern Adriatic associated with orographic triggering of convection and extensive stratiform rainfall.

2.1. SST data

In this study we used SST measured in-situ at a number of stations in Croatia and Italy (Figure 1), OSTIA and MUR analyses as well as ROMS model output. Data measured in situ are used to evaluate how well SST from different sources represents SST on eastern Adriatic, which contains numerous islands.

2.1.1. Operational SST

The initial SST fields used for the ALADIN operational forecast in 8 km and 2 km resolutions are taken from the initial file of the ARPEGE operational forecast. Action de Recherche Petite Echelle Grande Echelle (ARPEGE, Météo France (2012)) computes weather forecast on a stretched grid. So the horizontal resolution is variable over the globe, with the highest resolution over France. The LBC files are distributed on a Lambert conformal grid in horizontal resolution of 10.6 km. The ARPEGE operational SST analysis combines Advanced Very High Resolution Radiometer (AVHRR) satellite data and in situ measurements in the operational oceanographic model Mercator (Bahurel et al., 2004). However, in a case of operational failure there were some alternatives used. In situ SST reports by ships and buoys are combined with NCEP SST analysis or a previous analysis (from 6 hours before) (Météo France, 2012). If everything else fails, Reynolds global cimatology (1 degree resolution) or European Centre for Medium Range Weather Forecast (ECMWF) SST analysis (Lebeaupin et al., 2006) can be used.

2.1.2. Analyzed SST in 0.05 degree (6.5 km) resolution - OSTIA

The Operational Sea Surface Temperature and Sea Ice Analysis (OSTIA) analysis (UK Met Office, 2005; Donlon et al., 2012; Stark et al., 2007) is produced daily on an operational basis at the UK Met Office using optimal interpolation (OI) on a global 0.054 degree grid. As input, it uses satellite data from the AVHRR, the Advanced Along Track Scanning Radiometer (AATSR), the Spinning Enhanced Visible and Infrared Imager (SEVIRI), the Advanced Microwave Scanning Radiometer-EOS (AMSRE), the Tropical Rainfall Measuring Mission Microwave Imager (TMI), and in situ data from buoys. It is designed as support for the SST data assimilation into NWP models.

2.1.3. Analyzed SST in 0.01 degree (1 km) resolution - MUR

The Multiscale Ultrahigh Resolution (MUR) SST analysis is produced as near-real-time dataset (one day latency) at the Jet Propulsion Laboratory (JPL) Physical Oceanography Distributed Active Archive Center (DAAC) using wavelets as basis functions in an optimal interpolation approach on a global 0.01 degree grid (Chin at al., 1998; JPL MUR MEaSUREs Project, 2015). As input, it uses skin and subskin SST observations from the NASA Advanced Microwave Scanning Radiometer-EOS (AMSRE), the Moderate Resolution Imaging Spectroradiometer (MODIS) on the NASA Aqua and Terra platforms, the US Navy microwave WindSat radiometer, AVHRR and in situ SST observations from the NOAA.

2.1.4. ROMS model SST

Aside from SST analysies described before, SST from the Regional Ocean Modelling System (ROMS,Shchepetkin and McWilliams (2005, 2009)) is used over the Adriatic Sea with OSTIA analysis over the rest of the Mediterranean. ROMS is run for the Adriatic region (Janeković et al., 2014) using Adriatic forecasting System (AFS) AREG lateral boundary conditions at the open boundary in the Straint of Otranto that is in turn nested inside the Mediterranean Forecasting System (MFS,Oddo et al. (2006)). The model grid has 2 km spatial resolutin and 20 s-levels in the vertical. The vertical resolution is increased in the surface layers and bathyimetry is computed using Dutour Sikirić at al. (2009). Fresh water sources are computed using more realistic values (Janeković et al., 2014) than fromer climatology (Raicich, 1994), which overestimates river fluxes.

2.1.5. SST measured in situ

In this study we use SST measured in situ on a number of stations in Croatia and Italy. SST is measured on a number of stations on the Adriatic, including a number of stations on the islands (Figure 1). Most of the stations on eastern Adriatic coast are the regular "climate" stations, which measure SST in conventional way at 7, 14 and 21 hours local time (at 06, 13 and 20 UTC) each day. These stations are Božava, Sv Ivan na pučini, Komiža, Krk, Lastovo, Mljet, Opatija, Pula, Rab, Rabac, Senj, Šibenik, Split, Zadar, Dubrovnik, Hvar, Bakar and Cres (see locations in Figure 1, some names are abbreviated). Since SST does not change rapidly in time, these measured values are compared to the analyses at 06, 12 and 18 UTC.

Several automatic stations on the eastern Adriatic coast measure SST on buoys anchored close to the coastline with an hourly interval (Zadar, Mljet, Malinska, Opatija, Dubrovnik and Crikvenica, see location in Figure 1). On stations Zadar, Dubrovnik and Opatija, there were both, conventional and automatic measurements available.

There are operational SST measurements available for a number of stations in Italy from ISPRA (Italian National Institute for Environmental Protection and Research). SST measurements from the stations in Italy are mostly available with an hourly interval.

2.2. Meteorological model

The operational forecast (Tudor et al., 2013) is used as the reference. The forecast suite consists of 8 km resolution forecast up to 72 hours run twice per day from 00 and 12 UTC. The analysis for 8 km run is performed by 3DVar (Stanešić, 2011). The second component of the operational forecast is 2 km resolution run up to 24 hours run once per day. It stars at 6 UTC, using initial conditions interpolated from the 8 km resolution run without data assimilation.

2.2.1. Operational 8 km hydrostatic forecast using ALADIN System

The operational forecast is computed using ALADIN System. It is a spectral limited-area model (LAM) with a quadratic elliptic truncation (Haugen and Machenhauer, 1993) that ensures that the nonlinear terms of the model equations are computed without aliasing. The domain in 8 km resolution consists of 240x216 grid points, including an unphysical band of 11 points along northern and eastern boundaries needed for the biperiodization. The model equations are solved using semi-implicit semi-Lagrangian discretisation (Robert, 1982) and finite differences on 37 levels in the vertical with hybrid pressure type eta coordinate (Simmons and Burridge, 1981). This includes the stable extrapolation two time level, semi-implicit, semi-Lagrangian advection scheme (SETTLS, Hortal (2002)) with a second-order accurate treatment of the nonlinear residual (Gospodinov et al., 2001). Semi-Lagrangian horizontal diffusion (SLHD) (Váňa et al., 2008) is based on the physical properties of the flow. The operational physics parametrisations at the time includes prognostic TKE, cloud water and ice, rain and snow (Catry at al., 2007) and diagnostic scheme for deep convection (Geleyn et al., 1995). The model variables are coupled to a large scale model at the lateral boundaries using a relaxation scheme (Davies, 1976) in a zone, which

is 8 grid points wide. The global model data are available with a 3-hourly coupling interval that could be insufficient to capture rapidly moving storms (Tudor and Termonia, 2010; Tudor, 2015). The initial conditions are computed by combining 3DVar for the upper air fields and optimal interpolation for surface (Stanešić, 2011).

The operational package of physics parameterizations uses a simple microphysics scheme with prognostic cloud water and ice, rain and snow (Catry at al., 2007) with a statistical approach for sedimentation of precipitation (Geleyn et al., 2008). The ratio of evaporation and fall speed for liquid and solid precipitation is reduced (Tudor, 2013) to avoid excess precipitation as a consequence of fibrillations that arise due to stiffness. Prognostic TKE (Geleyn et al., 2006) scheme includes a contribution of the shallow convection (Geleyn, 1987). The exchange with surface (Noilhan and Planton, 1989) and the surface data assimilation (Giard and Bazile, 2000) use the Interaction Soil Biosphere Atmosphere (ISBA) surface scheme. The turbulent exchange at the sea surface uses different mixing lengths for momentum and heat (Brožkova et al., 2006) that are modified from Charnock (1955). The interpolation of wind, temperature and humidity from the lowest model level (about 17 meters above ground) to the heights of the standard meteorological measurement (10 and 2 meters above ground) is computed using a parameterised vertical profile dependent on stability (Geleyn, 1988).

2.2.2. Operational 2 km non-hydrostatic ALADIN forecast

A high resolution operational forecast run, uses ALADIN System with non-hydrostatic dynamics (Bénard et al., 2010) and a complete set of physics parameterisations, including the convection scheme (Tudor and Ivatek-Šahdan, 2010). It is often assumed that convection is resolved at 2km resolution. Since the model is spectral with quadratic truncation, the shortest resolved wave is 6km long. The convection scheme is a prognostic one (Gerard and Geleyn, 2005; Gerard, 2007) and it allows combining resolved and convective contributions in the grey zone (Gerard et al., 2009). This forecast is computed using initial conditions interpolated from the 6 hour forecast of the 8 km resolution forecast that starts at 00 UTC. It is initialized using scale selective digital filter initialization (SSDFI, Termonia (2008)). It also uses hourly LBCs from the 8 km resolution forecast runs for 24 hours, until 06 UTC on the next day. That allows comparison to precipitation data from the rain-gauges available in the high resolution network.

The 2 km resolution simulations are often regarded as explicitly resolving

convection and this implies that there is no parametrization of convection used (Lebeaupin et al., 2006). The shortest wave represented by the model dynamics in the quadratic truncation in 2 km resolution is acutally $3\Delta x$ or 6 km in wavelength. Therefore, we use the 3MT convection scheme to parametrize the unresolved portion of deep convection.

2.2.3. Precipitation data

Here we describe the precipitation data used for validation of numerical experiments. The observational data used here are from the network of stations that operate routine meteorological measurements in Croatia and those from abroad that are available through routine international exchange. Data from Slovenian stations are available through a bilateral collaboration agreement. In 2012 the Croatian rain-gauge network consisted of more than 500 stations reporting accumulated rainfall for the 24 hours from 06 UTC until the 06 UTC the next day. The precipitation data from SYNOP reports is used for other countries in the domain.

However, in situ data do not tell us much about the precipitation over the sea. In order to fill in this void, precipitation estimates from satellite data are used. Satellite derived precipitation data are used as provided from the Tropical Rainfall Measuring Mission (TRMM, Huffman et al. (2007)), in particular we use the 3-hourly precipitation data from 3B42RT product and computed 24-hourly accumulated rainfall for the period from 06 UTC to 06 UTC the next day. TRMM data are available from Giovanni web server interface (Acker and Leptoukh, 2007) on http://disc.sci.gsfc.nasa.gov. These data were used to subjectively evaluate the spatial destribution of precipitation, but not in the computations of statistical scores.

2.3. SST computations

The model has one field that describes the surface temperature (regardless the underlying surface) and another field that represents land sea mask (LSM), which can assume only two values: zero for sea/water surface and one for land. In the subsequent computations, surface temperature in the model is modified only for grid points where LSM is zero (sea points).

2.3.1. Introducing OSTIA and MUR SST analyses to ALADIN model fields

For each ALADIN model grid point with LSM equal to zero, one would look for the closest sea point in the OSTIA or MUR analysis of SST. If this point in the analysis is closer than a pre-defined distance, the SST value from

the analysis is used. If the closest point in the analysis is too far, the original operational value is kept (this prevents the procedure from modifying data on lakes).

This approach works fine for MUR analysis of SST that is in high resolution and has data over the southern portion of the VC. When introducing OSTIA SST analysis, this approach does not modify SST in the southern part of VC unless it also modifies SST over the Skadar Lake. The OSTIA SST analysis does not contain SST data over the southern VC. To make things worse, the closest sea point for the southernmost portion of VC is Zadar (in the south), not the northern part of VC.

While developing the procedure, an experiment forecast was done in which the procedure for incorporating OSTIA SST was modified so that southern part of VC uses SST from the northern part (the sea it is connected to) and not from the closest area (close to Zadar). This yields constant temperature over southern VC that has the same value as the closest point in Ostia.

2.3.2. Introducing ROMS model data to ALADIN model fields

The ROMS domain covers only Adriatic. So ROMS data are inserted in the SST field that is already modifield by values from OSTIA analysis. ROMS model SST data are used in the model so that for each ALADIN model grid point with LSM equal to zero, one would look for the closest point in the ROMS field and assign a value to the model SST that is computed as:

$$T_n = T_m + \frac{r_M - r_d}{r_M} (T_r - T_m) \tag{1}$$

where T_n is the new SST value, r_M is maximum radius of influence (tuning parameter that can smooth the transition at the edge of ROMS domain), r_d is the distance between the ALADIN and ROMS grid-points, T_r is SST from the closest point in ROMS and T_m is the ALADIN model SST in a grid point (already modified by OSTIA data). The above formula therefore uses the closest sea point on the ROMS grid. The same procedure can be used to smooth the transition of SST at otranto from ROMS to OSTIA data. Otherwise there would be sharp artificial gradients. $r_M = 0.25$ degrees is used in the experiments shown here.

2.3.3. Introducing in situ measurements of SST

As mentioned in the introduction, it was suggested that introducing in situ measurements into the SST field could inprove the precipitation forecast. One experiment tests this hypothesis for the HyMeX SOP1 period. The SST field, modifield by values from OSTIA analysis, is nudged towards SST values measured in situ. For each ALADIN model grid point with LSM equal to zero, one computes the distance to the closest point of measurement r_s. If this distance is less than a pre-defined value r_M, the new SST value is computed as

$$T_n = T_m + \frac{r_M - r_s}{r_M} (T_s - T_m) \tag{2}$$

where T_n is the new SST value, r_M is maximum radius of influence (tuning parameter that defines the area of influence of the point measurement), r_s is the distance between the ALADIN grid-point and the point of measurement, T_s is the measured SST from the closest station and T_m is the ALADIN model SST in a grid point. The above formula is applied only for the closest point of measurement and only if it is closer than $r_M = 0.5\ ^\circ$.

2.4. The intensive precipitation event in Rijeka during IOP2 in the evening of 12 September 2012

The effect of SST on IPEs is tested on the whole SOP1 period and on one particular IOP during SOP1. A heavy precipitation event occurred over the north-eastern Italy, Slovenia and north-west Croatia in the afternoon and evening of 12th September 2012 (Manzato et al., 2015; Ivančan-Picek et al., 2016). The event is associated to a warm and moist low level air-mass from the Adriatic Sea and a cold front. During the day, there were three storms, several hours apart, over northeast Italy including a supercell storm that developed in the morning (Manzato et al., 2015) over northeastern Italy. Nearby area of Istria and Rijeka received the first rainfall in the early afternoon, but precipitation soon stopped. Later in the evening, IPE occurred over northwest Croatia, particularly the city of Rijeka and surrounding area where several raingauges measured more than 200 mm of precipitation in 24 hours. According to the raingauge in Rijeka, the torrential rain in the evening fell during 2 hours between 21 and 23 UTC. It was connected to the last storm over Italy (Manzato et al., 2015) that was moving along the coast of north Adriatic over Istria towards Rijeka and Kvarner. During the day, moist air over the central Adiratic became saturated. Convection developed

over the northern Adriatic and warm and moist advection produced intensive precipitation triggered by the orography. The flash floods occurred during the night and caused substantial damage.

This IPE event was predicted by ALADIN operational forecasts in 8 km resolution with precipitation exceeding 100 mm inland of Rijeka, but still underestimated 220 mm that was actually measured. This event is studied in more detail in Ivančan-Picek et al. (2016). Here we show that the position of maximum precipitation in the operational forecast was shifted inland from Rijeka due to too warm SST in Kvarner and Rijeka Bay and VC.

3. Results

In this section we first analyze the SST fields obtained by the procedure described above and used in subsequent experiments. The fields are illustrated for one day, 12 September 2012 to show how the spatial variability changes. Then, we compare the the SST measured in situ to the values of SST fields in the closest sea point in the model used in different experiments for the whole SOP1 period. Afterwards, the precipitation forecasts from different experimetns are evaluated. The experiments consisted of running 61 forecasts for up to 72 hours in 8 km resolution. In each experiment SST was modified as explained in Table 1 and previous section. The results of experiments in 8 km and 2 km resolution are here discussed and illustrated for one case of IPE in Rijeka on 12 September 2012.

3.1. Qualitative evaluation of SST fields

In 2012, the data in the coupling files of ARPEGE was in 10.6 km resolution. The SST value in the initial file of the 8 km resolution forecast is modified using SST from different sources as described in the Subsection 2.3.

We compare the SST fields for one day during HyMeX SOP1 first, as an example of differences found on daily basis. Some inconsistencies in SST provided in the files could be attributed to low resolution of the global analyses and/or vicinity of the coastline. The operational SST taken from ARPEGE for 12 September 2012 (Figure 2a) shows a cold pool (20-22°C) spreading from the Bay of Lyon, a warm pool (28-29°C) around Sicilly and in Ionian Sea, while the rest, including Adriatic, is in the range from 24°C to 27°C. The SST is particularly warm in a narrow area close to Cotě d' Azur and SST

field is rather warm and smooth over the Adriatic (24-26°C). SST used operationally is colder by 1-2 K than any alternative SST for southern Adriatic and Ionian Sea.

On the other hand, SST from OSTIA analysis is colder over most of the Western Mediterranean and Aegean Sea (Figure 2 b and c) by 1 to 3 °C with an exception of the Ionian Sea, the central part in the southern Adriatic and few spots in the western Mediterranean. There is a cold pool in north-east Adriatic and the cold pool spreading from the Gulf of Lyon is few degrees colder than in ARPEGE and there is no warm belt along the Cotě d' Azur. The SST field from OSTIA has larger spatial variability with several cold pools.

The ROMS model output is available for the Adriatic and used to modify SST, which is already modified by OSTIA. The resulting SST field has high spatial variability over the Adriatic with large spatial gradients (Figure 2 d and e). The SST is colder along eastern coastline, particularly between Istria and Velebit mountain and in southeast Adriatic close to the outlet of Bojana river, and slightly colder in the area close to Venice. ROMS SST is the highest (when compared to SST analyses) in the central parts of middle and southern Adriatic, away from the coastline. ROMS is actually much warmer than OSTIA over most of the Adriatic region (except close to coast in the southeast) and the cold pool in the northeast is less spatially extensive with larger temperature in Kvarner Bay, but lower in VC and Rijeka Bay. However, ROMS also contains SST data over the southern VC that is considerably colder (several °C) than the surrounding sea.

The MUR analysis provides SST in the highest resolution and the procedure applied here does not apply smoothing to it. Resulting SST has higher spatial variability than the operational SST from ARPEGE and OSTIA analysis (Figure 2 f and g). Just as OSTIA, the SST from MUR is colder than operational ARPEGE with an exception of southern Adriatic and several patches over western Mediterranean and the warm tounge of SST along Cotě d' Azur is non-existent. The cold pool in northeast Adriatic is less intensive than in ROMS and less spatially extensive than in OSTIA. The southern part of VC is also warmer than in ROMS.

In 2km resolution operational run that uses SST from ARPEGE, SST has low spatial variability (Figure 3). When SST from OSTIA is used, SST is much lower in coastal areas; Kvarner Bay, Trieste Bay etc. SST in the southern part of VC is left unchanged with respect to the operational one. The differences in SST exceed 4K. SST from ROMS has highest spatial vari-

ability and coldest values in the southern part of VC and southeast Adriatic (between Montenegro and Albania). On the other hand ROMS is warmest over the open sea of central and southern Adriatic. The differences between OSTIA and ROMS are the largest on the eastern side of Adriatic where SST from ROMS is lower.

The Figure 3 shows results for ROMS with large R_r when SST of Skadar Lake was also modified using values from the sea nearby. This is because the same procedure was used to smooth the transition from ROMS SST to OSTIA SST at the straight of Otranto. ROMS SST fields shows dynamical features of the Adriatic sea such as eddies and filaments and interchanging tongues of warm and cold sea and SST exhibits sharp gradients. Other SST fields used here are smoother. Operational and OSTIA SST are smoother due to resolution. MUR SST analysis is in higher spatial resolution than ROMS but the field is smoother and much warmer along the eastern Adriatic coastline than ROMS. All alternative SST fields have higher values than operational for central and southern Adriatic and lower values along coastlines.

All SST fields show colder SST along the eastern Adriatic than the middle and the western side. This is a bit different situation than what is usually found. The eastern Adriatic current is bringing warm water from the Ionian Sea. While the western Adriatic current flows southeastward and is usually colder than the rest of the Adriatic. The strong, cold and dry bura wind from the eastern shore can cool the sea surface by several degrees in a day. The sea evaporates intensively and looses heat due to latent heat consumption. Strong wind also enhances mixing of the sea in vertical.

3.1.1. Point-based comparison of SST to in situ measurements

Here we compare the model SST in the modified initial fields with the values measured on the stations. The operational SST used in the comparison is taken from the nearest sea point in the coupling file from ARPEGE. Since the coupling files contain data in 10.6 km resolution on a Lambert conformal grid, which is not native to the ARPEGE global model, there is already some horizontal interpolation involved when the files are created in Météo France and we want to avoid any additional interpolation. The SST in the forecast coupling files is the same as in the initial file. Therefore, the SST is taken only from the analysis fields of ARPEGE on 10.6 km resolution grid.

On the other hand, the SST from OSTIA and MUR analyses are introduced to the 8 km resolution intial fields that are on a Lambert conformal

grid using a procedure described in Chapter 2. The SST data from ROMS and in situ measurements are used to modify the SST field that is already modified by OSTIA on the same 8 km resolution grid.

Unlike the ARPEGE, the SST data for OSTIA, MUR and ROMS, which are used in the comparison are taken from the nearest sea point in the initial file of ALADIN on 8 km resolution grid. Since we simply overwrite the value of model SST by the values from OSTIA or MUR analyses (if the corresponding point is a sea point), there is no interpolation involved and the SST values are in fact equal to the closest sea point in the analyses.

The data from the nearest sea point is taken to evaluate the SST provided in the coupling files from ARPEGE for a number of stations where in-situ measurements of SST are available. The measured data are plotted against SST values from the nearest sea point for the period from 1 September to 10th November 2012 (Figure 4). The measured data are not smoothed for the diurnal cycle of SST. The ARPEGE and ROMS data also have a diurnal cycle, while analyses have one daily value. We do not compute errors here, but we try to identify when and where the differences between measured values and those from model/analyses are the largest. The Figure 4 reveals several characteristics:

- On most stations, there is an agreement in temporal changes in SST on long time scales even for several stations with complex coastline and surrounded by islands unresolved in global models.

- Measured SST shows larger temporal variability than the analyses and models. The difference between measurements and reanalysis/model data is often lower than the amplitue of the diurnal cycle in SST.

- On Senj and Bakar stations, measured SST is lower and far more variable than in analyses, possibly due to local ocean dynamics and local atmospheric features, such as cold and dry bura wind, which rapidly cools the sea surface.

- ROMS reproduces the cooling event on 12-14 September 2012, although it slightly underestimated the reduction of SST on both sides of Adriatic.

- MUR and OSTIA reproduce the same cooling event on the western coastline (although slightly underestimated by OSTIA), underestimate

the cooling at Trieste, but there is only a hint of the cooling at Senj and Bakar on the eastern Adriatic coastline.

Although we compare SST fields from the closest sea point and in-situ measurements that are done on the coastline, there is a good agreement in measured and model SST for the most of the stations.

SST changes on a scale of several weeks are represented in ARPEGE. Events with rapid cooling of SST of local character (such as for Senj and Bakar on 12 September 2012, Figure 4) are not represented in the changes in the SST provided from ARPEGE, and for several locations these cooling events are underestimated by the analyses. Measurements of SST on several stations exhibit similar intensive variations that are not present in SST data from analyses but these changes are represented in the ROMS model output.

The comparison of measured and operationally used SST reveals a significant bias. These differences can be substantial, especially in Rijeka Bay and VC (see stations Senj, Bakar, Rabac and Malinska in Figure 4). These areas are much colder than the rest of the Adriatic sea during HyMeX SOP1. This is not resolved in the SST fields from ARPEGE and OSTIA, while MUR analysis is warmer than in situ measurements. The area is small and contains many islands close to the coastline. It is not surprising that the cold pool is missed in the SST fields presented with the resolution of the global NWP model. This cold area has an impact on the local weather and on the meteorological parameters measured on the coastline, especially 2 m temperature and humidity. Using SST from a high resolution analysis or ocean model forecast, where these islands are resolved and well represented, could have a positive impact on the overall forecast performance. However, the comparison to measurements reveals that the cold pool between Istria and Velebit mountain is actually better represented in OSTIA than in MUR analysis.

The SST fields from ARPEGE do show that sea surface is slightly colder close to the Italian coast of Adriatic than at the open sea, but in-situ measurements show much colder sea surface there. This cold area is probably too narrow to be resolved by the global model ARPEGE and therefore colder Western Adriatic Current (WAC) is not present. It is possible that there are other high-resolution features in SST that are not well represented in the data used by the global NWP models. This cold sea current considerably affects 2 m temperature and humidity measured on meteorological stations nearby, which in turn could be rejected in the subsequent procedure for data assimilation.

3.2. Impact of changes in the SST on precipitation forecast

The impact of SST on the intensity and location of intensive rainfall is investigated. The operational run at the time of HyMeX SOP1 is driven by ARPEGE forecasts as lateral boundary conditions and SST is taken from the initial file of ARPEGE. In the first set of experiments, SST effects on forecast precipitation are analyzed by modifying the SST field in the initial file by shifting the SST field uniformly. For each model forecast, the initial SST field is modified by increasing or decreasing SST values by 2° and 5° and finally decreasing by 10° for all sea points in the model domain (see Table 1 for the list of experiments). These values are chosen on the basis of evaluation of model and analyzed SST against in situ data since the differences between measured and model SST reach and on several stations even exceed these values.

Precipitation accumulated over 61 days (Figure 5) from raingauge measurements is lower than the TRMM estimate. The accumulated precipitation during 61 days of SOP1 from raingauge measurements (Figure 5 left) shows a maximum extending from Kvarner bay to the Alps on the border between Austria, Italy and Slovenia. However, these measurements are done only over land and can be relatively sparse there, with vast areas of no data. The precipitation accumulated from the TRMM estimate for the same period (Figure 5 right) shows a secondary maximum over the southeast Adriatic, over the Montenegro coast, as well as over Ionian Sea. The latter shows several local maxima over the sea surface that are not present in the raingauge data (because of the absence of in situ measurements there). Here we can not determine if TRMM overestimates or the raingages underestimate precipitation (or both!), especially for the wide areas with no measureents (such as the sea surface). The TRMM data represent precipitation activity at a resolution of 0.25 degrees, which is coarser than the NWP models runs employed here. The raingauge data are known to underestimate the precipitation amounts due to high wind. The precipitation amounts from raingauges are not corrected for this (due to absence of measured wind speed at the location of many of the rain-gauges).

3.3. Results of experiments with uniform shift of SST

Here we analyze the rainfall produced by experiments when the operational SST (from ARPEGE) is increased or reduced by a fixed number. The analysis of the 8 km resolution experiments is performed for the first day (precipitation accumulated from 06 to 30 hour forecast) and the second

day (from 30 to 54 hour forecast). All experiments in 8 km resolution start from the 00 UTC analysis and only SST is modified. The precipitation from the first 6 hours of the forecast is ommitted from the analysis. The experiments in 2 km resolution start from the 6 hour forecast of the corresponding experiment in 8 km resolution.

3.3.1. Precipitation in 8 km resolution

The precipitation accumulated during 61 days of SOP1 from ALADIN forecasts in 8 km resolution shows abundant precipitation along the eastern Adriatic, especially over the inland mountains (Figure 6). Most of this precipitation is resolved with peaks of resolved precipitation over mountains. Convective precipitation is less intensive with intensity peak over the coastline and the sea surface. Over land, stratiform precipitation is more intensive than the convective precipitation, while the opposite can be said for the sea surface, where convective precipitation dominates.

The forecast precipitation peaks are located over mountain peaks and ridges, where no in situ measurements are available, but these precipitaton amounts can be seen in the TRMM data (Figure 5 right). The operational precipitation maxima over the sea (Figure 6) surface are much lower than the values from TRMM data, especially over the Tyrhennian Sea. It requires a substantial increase in the SST to reproduce that amount of precipitation by the model, since only TP5K experiment reaches the amount given by TRMM (Figure 6 top right).

Increasing/decreasing the SST produces more/less precipitation over the sea surface for all experiments with uniform shift in SST (for the difference with TP5K see Figure 6). The increase is more pronounced in the output of the convective scheme (unresolved precipitation) than the stratiform (resolved) precipitation. Precipitation is also larger over most of the surrounding mountains (Apennines and Dinaric Alps). There is one exception. The Alpine slopes of the Po valley receive more precipitation when SST is lower (Figure 7). This enhanced precipitation is mostly from the stratiform (resolved) precipitation scheme (Figure 7). Both convective and stratiform schemes yield more rainfall on the northern slopes of the Po valley when SST is lower. It is expected to get less precipitation overall with lower SST because the colder sea surface evaporates less. But, the colder sea surface triggers less convection over the sea surface so more moisture reaches the Alpine slopes. There, precipitation can be convective or stratiform, triggered by warm land surface, convergence of moisture by mountain flow or

forced lifting upslope.

Operational SST over Ionian Sea is lowar than OSTIA and MUR analyses. Warm SST evaporates more and more convection is triggered. TRMM data show intense precipitation over Ionian Sea that is absent from the operational forecast. The reason for this could be low SST there. However, another precipitation peak in TRMM data is over Tyrhennian Sea that is also underestimated by the operational forecast. But operational SST is higher than in the analyses so underprediction of precipitation there could not be explained by low SST.

3.3.2. Precipitation in 2 km resolution

The 2 km resolution forecast produces higher precipitation maxima than 8 km forecast over the mountains along the eastern Adriatic (Figure 8). The mountain peaks and ridges are higher in increased horizontal resolution and the slopes are steeper. Most of this enhanced precipitation intensity arises from the convection scheme (Figure 8), especially for the seaward slope of the mountains. The local maximum of resolved precipitation is over the ridge of the Velebit mountain while the maximum intensity of the convective precipitation is on the slope facing the sea (VC). There is also more convective than stratiform precipitation over the sea surface.

Comparing the precipitation forecastsi in TM5K and TP5K experiments (with decreased and increased SST) shows that when SST is lower the precipitation decreases over most of the domain, with an exception ofi southern Alpine slopes and an area between Ortona and Ancona. Both resolved and convective precipitation increase on the southern slopes of Alps (north of Po valley). As already mentioned in the discussion of the results of experiments in 8 km resolution, lower SST triggers less convective precipitation over the sea surface so more is left to precipitate ofe the Alpine slope. Lower SST precipitation slightly inreases in the area between Ancona and Ortona in Italy due to enhanced resolved precipitation and little change in the convective precpitation. There is similar effect in 8 km resolution forecast (Figure 6). When SST is reduced, the precipitation over Velebit mountain shifts from convective to stratiform. Consequently, there is more stratiform precipitation over Velebit in TM5K experiment than in TP5K experiment. The stratiform precipitation is enhanced but the convective is reduced even more so the overall effect of reducing SST on the precipitation amount is negative on that location.

Operational SST is very smooth and misses several high resolution fea-

tures. It contains errors that are not uniform in space. Shifting SST by a fixed value keeps the horizontal gradients of SST unaltered. On the other hand, the gradient between sea and land surface temperature did change substantially. The gradients in SST used operationally are lower than in fields from SST analysis and the ocean model.

The colder sea surface evaporates less so less moisture enters the atmosphere. Therefore, it is expected to have less precipitation when the sea surface is colder. When the sea surface is warmer, evaporation is more intensive and the atmosphere receives more moisture, the atmosphere produces convection and more precipitation is triggered over the sea surface. On the other hand, more stable (but stil moist) air does not precipitate (as much) over the sea surface, but carries the moisture over the valley towards the Alpine slopes. The stable air is forced upslope and precipitates mostly through the resolved upward motions or triggered by moisture convergence. In TM5K experiment, cold but moist air moves from colder sea surface to warmer land surface. More precipitation is triggered when this moist air is forced upslope and not over the flat Po Valley before the mountain.

3.4. Results of experiments with SST from analyses and ROMS

Here we analyze the precipitation in experiments where operational SST was repalced by SST from OSTIA, MUR and ROMS. As for the uniform shift experiments, we compare the results accumulated during 61 days of HyMeX SOP1 of the 24 hourly precipitation. All experiment start from the same analysis with modified SST.

3.4.1. Precipitation in 8 km resolution

There is more precipitation in the operational forecast than in any of the experiments (OSTIA, ROMS, MUR, MEAS) over western Mediterranean (10-50 mm over 61 days) due to increase in convective precipitation (Figure 7) with negligible differences in results between different experiments (results are shown onlyfor the ROMS experiment). The operational forecast used warmer SST there which in turn enhanced convection over warmer sea surface. However, OPER has slightly more rain over lateral parts of Ionian Sea where SST was lower than in other experiments, probably due to advection of moisture from neigbouring areas (warmer seas). Over Adriatic and Otranto, there are interchanging areas of positive and negative precipitation differences (positive means OPER yields more precipitation). That suggests a shift of precipitaton northward (downstream for most of the precipitation

cases here) in the Otranto Straight in OPER with respect to OSTIA and westward (and from land to the sea surface) in MUR. In both experiments, SST was colder in OPER there. Precipitation in the southeast Adriatic decreases more in the ROMS experiment due to existence of a cold pool of SST in that area during part of SOP1. However, OPER yields less precipitation over central and southern Adriatic than ROMS (Figure 7) with lower differences for OSTIA and MUR. Both resolved and convective precipitation are lower in the OPER experiment than in ROMS experiment. SST over most of the central and southern Adriatic (away from coastlines) was substantially warmer in ROMS. This enhanced evaporation, triggered more precipitaton above the sea surface and also brought more moisture to the coastal areas to the north. Most of the Northern Adriatic receives more rainfall in the OPER experiment, especially the area of Kvarner, where the differences in SST were also the largest. However the most northwest part, around Venice and stretching inland, actually received less precipitation in the OPER experiment, although SST there was also higher (in OPER than in other experiments). The differences in convective precipitation are mostly limited to the sea surface and nearby mountains. The impact of SST on the stratiform precipitation reaches further inland, especially for the area east of the Adriatic coast. The influence of SST spreads more than 200 km from the shore although there are many mountains on the way.

3.4.2. Precipitation in 2 km resolution

The precipitation from different experiments is accumulated during 61 days of HyMeX SOP1 and its differences with respect to the reference are shown in Figure 9 (reference minus experiment is shown meaning that positive values mean more precipitation in the reference run and negative values mean more precipitation in the experiment). The local intensity of precipitation can be substantially different, exceeding 200 mm (both negative and positive values in Figure 9). However, an area with positive precipitation difference is usually adjacent to an area with a negative difference. This means that precipitation has slightly shifted. The exceptions are an area stretching southward of Rijeka and southeastern Adriatic where reference yields substantially more precipitation due to warm SST. The impact of SST change on convective precipitation reaches further inland than for 8 km resolution forecast because the 2 km forecast uses a prognostic convection scheme. Precipitation forecast in 2 km resolution is more sensitive to SST than the 8 km resolution forecast.

3.5. Surface fluxes

Figure 10 shows surface temperature, 2 m temperature and relative humidity and wind speed from model forecasts in 2 km resolution during HyMeX SOP1. The values are averaged over a square with corners at longitude and latitude coordinates SW (14.7,44.7) NE (15.0,45.2) using only values over the sea points.

Figure 11 shows total fluxes of heat (sensible+latent), turbulent flux of momentum and total water flux (precipitation + evaporation) from model forecasts in 2 km resolution during HyMeX SOP1. The values are averaged over a square with corners at longitude and latitude coordinates SW (14.7,44.7) NE (15.0,45.2) using only values over the sea points.

Surface fluxes are more intensive with higher SST. Heat fluxes from the ocean to the atmosphere (taken negative in Figure 11) increase twofold from ROMS experiment (with coldest SST, see Figure 10) to experiment TP2K. The effect of SST change on other fluxes is less dramatic. Turbulent fluxes of momentum also increase with rising SST (Figure 11) but the differences are more subtle. Both evaporation (negative water flux in Figure 11) and precipitation increase with higher SST so that precipitation is more intensive during IPEs and evaporation is more intensive during bura events.

3.6. Impact on precipitation for IOP 2

Here we show results for one case of IPE during HyMeX SOP1. Out of 8 cases of IPE that affected eastern Adriatic coast during SOP1, 6 of them affected Rijeka area (Ivančan-Picek et al., 2016) so this case is chosen to represent the effect of changing SST to IPE. The reference experiment in the 8 km resolution is the operational forecast. For the whole period of HyMeX SOP1, operational forecast in 8 km resolution does simulate well developed convective systems, which are rich in moisture and generously pouring precipitation over different parts of eastern Adriatic coastline. The reference run simulates the meteorological envirnoment and the development of the convective system for each case, but success of the precipitation forecast varies between cases and consecutive forecast runs.

The location of precipitation maximum in the operational forecast is situated more inland than the observed one. In order to distinguish the contribution of the change in SST from other factors, all experiments start from the operational analysis and only SST values are modified. The same initial conditions are used for the operational run and all experiments, except the SST that was modified using data from different sources. The temperature

and moisture on the lowest levels in the atmosphere remain the same as for the initial conditions in the operational forecast and adapt to the new SST conditions during the forecast run. Lower SST moves the precipitation upstream and closer to the coastline while higher SST moves precipitation higher on the mountain slopes. Lower SST stabilises lower layers of the atmosphere so moist air has less energy to ascend the slope before releasing precipitation.

The operational run starting from the 00 UTC alaysis on 11 September 2012 does forecast the position of maximum precipitation correctly (Figure 12). Subsequent operational forecasts are less successful in forecasting the position of precipitation maximum and move it nortwest. The accumulated 24 hourly precipitation and its differences between experimetns are shown for the 2nd day of simulation (precipitation is accumulated from 30 to 54 hour forecast that started at 00 UTC of the previous day, Figure 12). When SST from analyses or ocean model is used (result for ROMS experiment is shown), the spatial distribution of precipitation is very similar to the operational forecast. The main factor determining the precipitation pattern in this case is the atmospheric flow and the mountains. However, the plot showing the difference between the two precipitation fields (Figure 12, center right) reveals that the precipitation maximum actually shifts southeastward (upstream). This small shift in the location of precipitation maximum exists already in OSTIA experiment. This shift contributs to local increase of precipitation in Rijeka and Kvarner Bay. The local precipitation maximum in Rijeka and Kvarner is further enhanced in ROMS experiment (Figure 12, bottom left). Consequently, ROMS experiment enhances precipitation over Kvarner Bay more than OSTIA (ROMS is colder there than OSTIA, while OSTIA is already colder than ARPEGE SST). Using MUR analysis (Figure 12, bottom right) has a similar effect as OSTIA. Nudging OSTIA SST towards in situ measurements has rather small effect (not shown). The precipitation band in MUR experiment is not only shifted upstream, precipitation is more concentrated in a narrow band stretching southeast from Rijeka on its northwest end. Finally, TRMM data (Figure 12 top left) show more rain over central Adriatic than predicted by any experiment.

The high resolution reference forecasts precipitation maximum over Rijeka and inland (Figure 13). This run uses initial and lateral boundary conditions from the operational 8 km resolution run from 00 UTC 12 September 2012. That particular 8 km resolution run put the maximum precipitation over Slovenia and northeastern Italy. One can interpret this improvement in

localization as a benefit gained by higher resolution and better representation of topography and islands. In the experiments with alternative SSTs, precipitation pattern is rather similar. The differences in precipitation reveal that part of the precipitation shifts 20-50 km, yielding stripes in the precipitation difference. As expected, the differences are the largest at locations of precipitation maxima, such as at the border between Slovenia and Italy and inland of Rijeka and exceed 50 mm/24 hours (both positive and negative). The river catchments in the area are rather narrow, hence this shift affects which river catchment is expected to receive excess precipitation.

3.7. Categorical verification

In this section, statistical parameters are computed using data measured in situ (TRMM data are ommitted). The precipitation data is divided into three categories. An event is defined as dry if the 24 h accumulated precipitation on the rain gauge station is less than or equal to 0.2 mm. The threshold between medium and strong rainfall is determined as 95^{th} percentile during the whole SOP1 period at all available stations (the dry events are excluded), which is equal to 50.42 mm accumulated in 24 hours. During the SOP1, the dry category has the highest base rate (BR), while strong precipitation is quite rare (happens only in 1.8% occasions, Table 2).

The OPER ALADIN 8 km forecast overestimates the frequency of medium precipitation category, while the frequencies are underestimated for the other two categories. The overforecast of medium and underforecast of the dry category is even more evident for OSTIA, MUR and ROMS. On the other hand, OSTIA and MUR overestimate the frequency of strong precipitation, while ROMS predicts this category almost as often as it occurs. The Critical Success Index (CSI) is the highest for the most common category (dry), and this is the direct consequence of the sensibility of this measure to underlying climatology. The medium precipitation events seem to be the best detected, due to overforecast of this event. Also, the category of the strong precipitation seems to be the hardest one to predict, with the smallest probability of detection, as well as the highest false alarm rate (FAR). But, if the results for different SST are compared, it can be seen that the best results are achieved for OPER. Even though OSTIA, MUR and ROMS predict the strong (and medium) category more often and increase probability of detection (POD), they also increase the FAR. Consequently, the CSI is actually smaller if compared to OPER.

In the experiments, only the initial SST is modified while the rest of the atmosphere adapts to this condition during the forecast. It takes (forecast) time to adapt. The tuning of operational LAM used here was done using the operational SST from ARPEGE (including the convection triggering). Consequently, the spatial distribution of precipitation seems better when assessed subjectively, and new SST field is more realistic, even though the differences in verification measures are small. The differences in the accumulated precipitation over 61 days are small compared to the total amounts. The verification measures are highly sensitive to the errors in space and time. There are considerable areas with no in situ measurements.

The differences between OPER, OSTIA, MUR and ROMS are much smaller for ALADIN 2 km (Table 4) than for ALADIN 8 km forecasts. This means that ALADIN 2 km is less sensitive to perturbations of SST. The OPER ALADIN 2 km is less biased than OPER ALADIN 8 km for all categories. Due to higher FB than for ALADIN 8 km, ALADIN 2 km has higher POD and FAR for dry category, while for medium category FB, FAR and POD are smaller. In general, the CSI value is the same or higher for ALADIN 2 km than for ALADIN 8 km forecasts. This shows that by increasing the resolution of the model and improving physics all the events are more accurately predicted, regardless of their BR. If compared to OPER, by modifying the SST for ALADIN 2 km forecasts, FB changes only for strong precipitation category. For modified ALADIN 2 km forecasts, the strong precipitation FB is the closest to 1 for ROMS SST, but still overestimating the frequency of strong precipitation more than for ALADIN 8 km forecasts. The smaller the FB in OSTIA, MUR and ROMS SST ALADIN 2 km forecasts, the smaller the POD, while FAR is almost the same. This means that modification of SST in these cases reduces the frequency of forecasted strong precipitation events, but also reduces the correctly forecasted ones.

4. Summary and conclusions

Adriatic sea is surrounded by mountains that often receives substantial amounts of precipitation in short time (24 hours). These heavy precipitation events are a result of air-sea interactions and influence of mountains on atmospheric flow.

Here we analyse the influence of sea surface temperature (SST) on IPEs during HyMeX SOP1. The effect of SST on intensity and location of precipitation maxima is explored in 8 and 2 km resolution on IPEs that affect the

coastline of the eastern Adriatic. The location of maximum precipitation is more dependent on SST than the cases analyzed in Davolio et al. (2016).

In the experiments with uniform shift of SST, the overall precipitation did increase/decrease with the increase/decrease of SST. More detailed analysis shows that this is mostly due to the increase of convective precipitation over the sea surface and stratiform on the surrounding mountains. However, the southern Alpine slopes facing the Po valley actually receive less precipitation when SST increases. This is probably because more convection is triggered over the sea surface (due to warm surface), leaving less moisture to precipitate when reaching the mountain slope. In 2 km resolution, another effect can be seen on the Velebit mountain. When SST is decreases, precipitation changes from convective to stratiform, and the total precipitation is reduced. Colder sea surface evaporates less, triggers less convection and gives less buoyancy to the air parcel above.

The situation is different in the Kvarner bay because there is no valley on the shore of the eastern Adriatic before the mountains. The existence of cold air pool depends on the SST in Kvarner Bay that is much warmer in operational atmospheric model than in reality. This sea surface also contains several islands that pose substantial topographic obscacles for the low level flow. Colder sea surface in the Kvarner Bay and VC contributes to enhanced precipitation over Rijeka area.

The air parcel attained buoyancy through condensation and released condensates through precipitation. Higher SST yields more precipitation over the sea surface, especially more convective precipitation. Lower SST reduces precipitation by reducing convection, particularly the most intensive one.

Acknowledgements. The Group for High Resolution Sea Surface Temperature (GHRSST) Multi-scale Ultra-high Resolution (MUR) SST data were obtained from the NASA EOSDIS Physical Oceanography Distributed Active Archive Center (PO.DAAC) at the Jet Propulsion Laboratory, Pasadena, CA (http://dx.doi.org/10.5067/GHGMR-4FJ01). This work represents a contribution to the HyMeX international program. The support for the study was received by the Ministry of Science, Education, and Sports of the Republic of Croatia.

Acker, J.G., Leptoukh, G., 2007. Online Analysis Enhances Use of NASA Earth Science Data, *Eos, Trans. AGU,* Vol. 88, No. 2.

ALADIN International Team, 1997. The ALADIN project: Mesoscale modelling seen as a basic tool for weather forecasting and atmospheric research, *WMO Bull.,* 46, 317–324.

Bahurel, P, Dombrowsky, E., Lellouche, J.M., the Mercator Project Team, 2004. Mercator ocean monitoring and forecasting system, near-real time assimilation of satellite and in situ data in different

operational ocean models, paper presented at 36th Colloquim on Ocean Dynamics, Geohydrodyn. and Environ. Res. Group, Univ of Liége, Liége, Belgium.

Bénard, P., Vivoda, J., Mašek, J., Smolíkova, P., Yessad, K., Smith, Ch., Brožková, R., Geleyn, J.-F., 2010. Dynamical kernel of the Aladin-NH spectral limited-area model: Revised formulation and sensitivity experiments. Quart. J. R. Meteorol. Soc. 136, 155–169. DOI: 10.1002/qj.522.

Brožkova, R., Derková, M., Belluš, M., Farda, A., 2006. Atmospheric forcing by ALADIN/MFSTEP and MFSTEP oriented tunings. Ocean Sci., 2, 113–121.

Cassola, F., Ferrari, F., Mazzino, A., Miglietta, M. M., 2016. The role of the sea on the flash floods events over Liguria (northwestern Italy), Geophys. Res. Lett., 43, 3534–3542, doi:10.1002/2016GL068265.

Catry, B., Geleyn, J.-F., Tudor, M., Bénard, P., Trojakova A., 2007. Flux conservative thermodynamic equations in a mass-weighted framework, *Tellus, Ser. A,* 59, 71–79.

Charnock, H., 1955. Wind stress on a water surface. Quart. J. Roy. Meteorol. Soc. 81, 639–640.

Chin, T.M., Milliff, R.F., Large, W.G., 1998. Basin-scale, high-wavenumber sea surface wind fields from a multiresolution analysis of scatterometer data. Journal of Atmospheric and Oceanic Technology, 15, 741-763.

Davies, HC., 1976. A lateral boundary formulation for multi-level prediction models. Quart. J. R. Met. Soc. 102 : 405 - 418. DOI:10.1002/qj.49710243210.

Davolio, S., Stocchi, P., Carniel, S., Benetazzo, A., Bohm, E., Ravaioli, M., Riminucci, F., Li X., 2015. Exceptional Bora outbreak in winter 2012: Validation and analysis of high-resolution atmospheric model simulations in the northern Adriatic area, Dynam. Atmos. Oceans, 71, 1–20.

Davolio, S., Volonté, A., Manzato, A., Pucillo, A., Cicogna, A., Ferrario, M. E., 2016. Mechanisms producing different precipitation patterns over North-Eastern Italy: insights from HyMeX-SOP1 and previous events, Q. J. Roy. Meteor. Soc., doi:10.1002/qj.2731.

Donlon, C. J., Martin, M., Stark, J., Roberts-Jones, J., Fiedler, E., Wimmer, W., 2012. The operational sea surface temperature and sea ice analysis (OSTIA) system, Remote Sens. Environ., 116, 140–158.

Dutour Sikirić, M., Janeković, I., Kuzmić, M., 2009. A new approach to bathymetry smoothing in sigma-coordinate ocean models, Ocean Modell., 29, 128-136.

Doswell, C.A., Brooks, H.E., Maddox R.A., 1996. Flash flood forecasting: An ingredients-based methodology, *Wea. Forecasting,* 11, 560–581.

Drobinski, P., Ducrocq, V., Alpert, P., Anagnostou, E., Béranger, K., Borga, M., Braud, I., Chanzy, A., Davolio, S., Delrieu, G., Estournel, C., Filali Boubrahmi, N., Font, J., Grubišić, V., Gualdi, S., Homar, V., Ivančan-Picek, B., Kottmeier, C., Kotroni, V., Lagouvardos, K., Lionello, P., Llasat, M.C., Ludwig, W., Lutoff, C., Mariotti, A., Richard, E., Romero, R., Rotunno, R., Roussot, O., Ruin, I., Somot, S., Taupier-Letage, I., Tintore, J., Uijlenhoet, R., Wernli, H., 2014. HyMeX: A 10-Year Multidisciplinary Program on the Mediterranean Water Cycle. Bull. Amer. Meteor. Soc., 95, 1063–1082, DOI:10.1175/BAMS-D-12-00242.1.

Ducrocq, V., Braud, I., Davolio, S., Ferretti, R., Flamant, C., Jansa, A., Kalthoff, N., Richard, E., Taupier-Letage, I., Ayral, P.-A., Belamari, S., Berne, A., Borga, M., Boudevillain, B., Bock, O., Boichard, J.-L., Bouin, M.-N., Bousquet, O., Bouvier, C., Chiggiato, J., Cimini, D., Corsmeier, U., Coppola, L., Cocquerez, P., Defer, E., Drobinski, P., Dufournet, Y., Fourrié, N., Gourley, J.J., Labatut, L., Lambert, D., Le Coz, J., Marzano, F.S., Molinié, G., Montani, A., Nord, G., Nuret, M., Ramage, K., Rison, B., Roussot, O., Said, F., Schwarzenboeck, A., Testor, P., Van Baelen, J., Vincendon, B., Aran, M., Tamayo, J., 2014. HyMeX-SOP1, the field campaign dedicated to heavy precipitation and flash flooding in the northwestern Mediterranean. Bull. Amer. Meteor. Soc., 95, 1083–1100, DOI:10.1175/BAMS-D-12-00244.1.

Geleyn J-F., 1987. Use of a modified Richardson number for parameterising the effect of shallow convection. J. Met. Soc. Japan. Special 1986 NWP Symposium Issue, 141–149.

Geleyn, J.-F., 1988. Interpolation of wind, temperature and humidity values from model levels to the height of measurement. *Tellus, Ser. A,* 40, 347–351.

Geleyn, J-F., Bazile, E., Bougeault, P., Déqué, M., Ivanovici, V., Joly, A., Labbé, P., Piédeliévre, J-P., Piriou, J-M., Royer, J-F., 1995. Atmospheric parametrization schemes in Météo-France's ARPEGE NWP model. In Proceedings of the 1994 ECMWF seminar on physical parametrizations in numerical models. 385 - 402. ECMWF, Reading, UK.

Geleyn, J-F., Váňa, F., Cedilnik, J., Tudor, M., Catry, B., 2006. 'An intermediate solution between diagnostic exchange coefficients and prognostic TKE methods for vertical turbulent transport.' WGNE Blue Book.

Geleyn, J-F., Catry, B., Bouteloup, Y., Brožková, R., 2008. A statistical approach for sedimentation inside a micro-physical precipitation scheme. Tellus A 60 : 649–662. DOI: 10.3402/tellusa.v60i4.15375.

Gerard, L., 2007. An integrated package for subgrid convection, clouds and precipitation compatible with the meso-gamma scales. Quart. J. R. Met. Soc., 133, 711–730, DOI:10.1002/qj.58.

Gerard, L. and Geleyn, J-F., 2005. Evolution of a subgrid deep convection parametrization in a limited-area model with increasing resolution. Quart. J. R. Met. Soc., 131, 2293–2312, DOI:10.1256/qj.04.72.

Gerard, L., Piriou, J-M., Brožková, R., Geleyn, J-F., Banciu, D., 2009. Cloud and precipitation parameterization in a meso-gamma scale operational weather prediction model. Mon. Wea. Rev., 137, 3960 - 3977, DOI:10.1175/2009MWR2750.1.

Giard, D. and Bazile, E., 2000. Implementation of a new assimilation scheme for soil and surface variables in a global NWP model. Mon. Wea. Rev., 128, 997–1015, DOI:10.1175/1520-0493(2000)128.

Gospodinov, I., Spiridonov, V., Geleyn, J-F., 2001. Second order accuracy of two-time-level semi-Lagrangian schemes. Quart. J. R. Met. Soc. 127 : 1017–1033. DOI:10.1002/qj.49712757317.

Grisogono, B., Belušić, D., 2009. A review of recent advances in understanding the meso- and microscale properties of the severe Bora wind, *Tellus, Vol A,* 61, 1–16.

Haugen, J., Machenhauer, B., 1993. A spectral limited-area formulation with time-dependent boundary conditions applied to the shallow-water equations. Mon. Wea. Rev., 121, 2618–2630.

Homar, V., Romero, R., Ramis, C., Alonso, S., 2002. Numerical study of the October 2000 torrential precipitaton event over eastern Spain: Analysis of the synoptic scale stationarity, Ann. Geophys., 20, 2047–2066.

Hortal, M., 2002. The development and testing of a new two-time-level semi-Lagrangian scheme (SETTLS) in the ECMWF forecast model. Q.J.R. Meteorol. Soc., 128: 1671–1687.

Huffman, G.J., Bolvin, D.T., Nelkin, E.J., Wolff, D.B., Adler, R.F., Gu, G., Hong, Y., Bowman, K.P., Stocker, E.F., 2007. The TRMM Multisatellite Precipitation Analysis (TMPA): Quasi-Global, Multiyear, Combined-Sensor Precipitation Estimates at Fine Scales. J. Hydrometeorol., 8, 38–55.

Ivančan-Picek, B., Horvath, K., Strelec Mahović, N., Gajić-Čapka, M., 2014. Forcing mechanisms of a heavy precipitation event in the southeastern Adriatic area. Natural hazards. 72, 1231–1252. DOI:10.1007/s11069-014-1066-y.

Ivančan-Picek, B., Tudor, M., Horvath, K., Stanešić, A., Ivatek-Šahdan, S., 2016. Overview of the first HyMeX Special Observation Period over Croatia. Nat. Hazards Earth Syst. Sci. Discuss., doi:10.5194/nhess-2016-247.

Janeković, I., Mihanović, H., Vilibić, I., Tudor, M., 2014. Extreme cooling and dense water formation estimates in open and coastal regions of the Adriatic Sea during the winter of 2012, J. Geophys. Res. Oceans, 119, 3200–3218, doi:10.1002/2014JC009865.

JPL MUR MEaSUREs Project. 2015. GHRSST Level 4 MUR Global Foundation Sea Surface Temperature Analysis (v4.1). Ver. 4.1. PO.DAAC, CA, USA. Dataset accessed [2016-03-01] at http://dx.doi.org/10.5067/GHGMR-4FJ04.

Lebeaupin, C., Ducrocq, V., Giordani, H., 2006. Sensitivity of torrential rain events to the sea surface temperature based on high-resolution numerical forecasts, J. Geophys. Res., 111, D12110, doi:10.1029/2005JD006541.

Manzato, A., Davolio, S., Miglietta, M.M., Pucillo, A., Setvak, M., 2015. 12 September 2012: A supercell outbreak in NE Italy?, Atmos. Res., 153, 98–118, DOI:10.1016/j.atmosres.2014.07.019.

Mastrangelo, D., Horvath, K., Riccio, A., Miglietta, M.M., 2011. Mechanisms for convection development in a long-lasting heavy precipitation event over southeastern Italy. Atmos. Res., 100, 586–602, DOI:10.1016/j.atmosres.2010.10.010.

Mazzocco Drvar, D., Plačko-Vršnak, D., Tudor, M., Trošić, T., 2012. Flash-flood in Pula in the night between 24 and 25 September 2010. Cro. Meteorol. Jour., 47, 35–43.

Météo France, 2012. Joint WMO technical progress report on the global data processing and forecasting system and numerical weather prediction research activities for 2012. 22 pp. available at www.wmo.int.

Noilhan, J., Planton, S., 1989. A Simple Parameterization of Land Surface Processes for Meteorological Models. Mon. Wea. Rev., 117, 536–549, DOI:10.1175/1520-0493(1989)117.

Oddo, P., Pinardi, N., Zavatarelli, M., Coluccelli, A., 2006. The Adriatic basin forecasting system, Acta Adriat., 47(Suppl.), 169–184.

Pastor, F., Estrela, M.J., Penarrocha, P., Millan, M.M., 2001. Torreintial rains on the spanish Mediterranean coast: Modelling the errect of the sea surface temperature, J. Appl. Meteorol., 40, 1180–1195.

Raicich, F., 1994. Notes on the flow rates of the Adriatic rivers, Tech. Rep. RF 02/94, 8pp., CNR, Ist. Sper. Talassografico, Trieste, Italy.

Rebora, N., Molini, L., Casella, E., Comellas, A., Fiori, E., Pignone, F., Siccardi, F., Silvestro, F., Tanelli, S., Parodi, A., 2013. Extreme Rainfall in the Mediterranean: What Can We Learn from Observations?. J. Hydrometeor., 14, 906–922, DOI:10.1175/JHM-D-12-083.1.

Robert, A., 1982. A semi-Lagrangian and semi-implicit numerical integration scheme for the primitive equations. J. Meteor. Soc. Japan., 60, 319–325.

Romero, R., Ramis, C. Alonso, S., 1997. Numerical simulation of an extreme rainfall event in Catalonia: Role of orography and evaporation from the sea, Q.J.R.Meteorol. Soc., 123, 537–559.

Shchepetkin, A.F., McWilliams, J.C., 2005. The regional ocean modelling system: a split-explicit, free-surface, topography-following-coordinate oceanic model, *Ocean Model.*, 9, 347–404.

Shchepetkin, A.F., McWilliams, J.C., 2009. Correction and commentary on "Ocean forecasting in terrain-following coordinates: Formuation and skill assessment of the regional ocean modelling system" by Haidvogel et al., J. Comput. Phys., 227, 3565-3624, J. Comput. Phys., 228, 8985-9000.

Silvestro, F., Gabellani, S., Giannoni, F., Parodi, A., Rebora, N., Rudari, R., Siccardi, F., 2012: A hydrological analysis of the 4 November 2011 event in Genoa. Nat. Hazards Earth Syst. Sci., 12, 2743–2752, DOI:10.5194/nhess-12-2743-2012.

Simmons, A.J., Burridge, D.M., 1981. An Energy and Angular-Momentum Conserving Vertical Finite-Difference Scheme and Hybrid Vertical Coordinates. Mon. Wea. Rev. 109, 758–766.

Small, R.J., deSzoeke, S.P., Xie, S.P., O'Neill, L., Seo, H., Song, Q., Cornillon, P., Spall, M., Minobe, S., 2008. Air-sea interactio over ocean fronts and eddies. Dyn. Atmos. Ocean. 45, 274-319.

Stanešić, A., 2011. Assimilation system at DHMZ: development and first verification results. Cro. Met. Jour., 44/45, 3–17.

Stark, J.D., Donlon, C.J., Martin, M.J., McCulloch, M.E., 2007. OSTIA : An operational, high resolution, real time, global sea surface temperature analysis system., Oceans 07 IEEE Aberdeen, conference proceedings. Marine challenges: coastline to deep sea. Aberdeen, Scotland.IEEE.

Stocchi, P., Davolio, S., 2016. Intense air-sea exchange and heavy rainfall: impact of the northern Adriatic SST. Adv. Sci. Res., 13, 7–12.

Strazzo, S.E., Elsner, J.B., LaRow, T.E., Murakami, H., Wehner, M., Zhao, M., 2016. The influence of model resolution on the simulated sensitivity of North Atlantic tropical cyclone maximum intensity to sea surface temperature, J. Adv. Model. Earth Syst., 8, 1037–1054, doi:10.1002/2016MS000635.

Termonia, P., 2008. Scale-selective digital filter initialization. *Mon. Wea. Rev.*, 136, pp. 5246–5255.

Toy, M.D., Johnson, R.H., 2014. The influence of an SST front on a heavy rainfall event over coastal Taiwan during TiMREX, J. Atmos. Sci., 71, 3223–3249.

Trenberth, K.E., Shea, D.J., 2005. Relationships between precipitation and surface temperature, Geophys. Res. Lett., 32, 1–4.

Tudor, M., 2013. A test of numerical instability and stiffness in the parametrizations of the ARPÉGE and ALADIN models. Geoscientific model development, 6, 901–913.

Tudor, M., 2015. Methods for automatized detection of rapid changes in lateral boundary condition fields for NWP limited area models. Geoscientific Model Development, 8, 2627–2643.

Tudor, M., Ivatek-Šahdan, S., 2010. The case study of bura of 1 and 3 February 2007, *Meteorol. Z.,* 19 (5) 453–466.

Tudor, M., Termonia, P., 2010. Alternative formulations for incorporating lateral boundary data into limited-area models. Mon. Wea. Rev., 138, 2867–2882.

Tudor, M., Ivatek-Šahdan, S., Stanešić A., Horvath, K., Bajić A., 2013. Forecasting weather in Croatia using ALADIN numerical weather prediction model. In: Climate Change and Regional/Local Responses / Zhang, Yuanzhi ; Ray, Pallav (eds.). Rijeka, InTech, 59-88.

UK Met Office, 2005. GHRSST Level 4 OSTIA Global Foundation Sea Surface Temperature Analysis. Ver. 1.0. PO.DAAC, CA, USA. Dataset accessed [2016-04-28] at http://dx.doi.org/10.5067/GHOST-4FK01.

Váňa, F., Bénard, P., Geleyn, J-F., Simon, A., Seity, Y., 2008. Semi-Lagrangian advection scheme with controlled damping – an alternative way to nonlinear horizontal diffusion in a numerical weather prediction model. Quart. J. R. Met. Soc., 134, 523–537, DOI:10.1002/qj.220.

Weill, A., Eymard, L., Caniaux, G., Hauser, D., Planton, S., Dupuis, H., Brut, A., Guerin, C., Nacass, P., Butet, A., Cloché, S., Pedreros, R., Durand, P., Bourras, D., Giordani, H., Lachaud, G., Bouhours, G., 2003. Toward better determination of turbulent air-sea fluxes from several experiments, J. Clim., 16, 600–618.

Table 1: List of experiments.

experiment	Description
OPER	operational SST from ARPEGE
TM51	SST reduced by 5°C
TM2K	SST reduced by 2°C
TP2K	SST increased by 2°C
TP5K	SST increased by 5°C
TM10	SST reduced by 10°C
OSTIA	SST taken from OSTIA
ROMS	SST from ROMS over Adriatic and OSTIA elsewhere
MUR	SST taken from MUR
MEAS	SST from OSTIA nudged towards measurements

Table 2: Base rate (BR), frequency bias (FB), probability of detection (POD) or hit rate (HR), false alarm rate (FAR) mad critical success index (CSI) verification measures calculated for 24 hour accumulated precipitation and for ALADIN 8 km experiments (first row) for three categories (second row) for whole SOP1 period (5 September to 6 November 2012).

experiment	OPER			OSTIA			MUR			ROMS		
category	dry	medium	strong	dry	medium	strong	dry	medium	strong	dry	medium	strong
BR (%)	64.9	33.4	1.8	64.9	33.4	1.8	64.9	33.4	1.8	64.9	33.4	1.8
FB	0.78	1.45	0.61	0.73	1.53	1.12	0.73	1.52	1.07	0.73	1.52	1.01
POD/HR	0.76	0.94	0.25	0.71	0.92	0.28	0.71	0.92	0.27	0.71	0.93	0.26
FAR	0.03	0.35	0.59	0.02	0.39	0.75	0.03	0.39	0.74	0.02	0.39	0.74
CSI	0.74	0.62	0.19	0.70	0.58	0.15	0.70	0.58	0.15	0.70	0.58	0.15

Table 3: Base rate (BR), frequency bias (FB), probability of detection (POD) or hit rate (HR), false alarm rate (FAR) mad critical success index (CSI) verification measures calculated for 24 hour accumulated precipitation and for ALADIN 8 km experiments (first row) for three categories (second row) for whole SOP1 period (5 September to 6 November 2012) for IOP days only.

experiment	OPER			OSTIA			MUR			ROMS		
category	dry	medium	strong	dry	medium	strong	dry	medium	strong	dry	medium	strong
BR (%)	18.1	74.8	7.1	18.1	74.8	7.1	18.1	74.8	7.1	18.1	74.8	7.1
FB	0.29	1.20	0.61	0.23	1.17	1.16	0.25	1.17	1.10	0.25	1.18	1.04
POD/HR	0.24	0.95	0.31	0.18	0.91	0.34	0.19	0.91	0.32	0.20	0.92	0.32
FAR	0.16	0.21	0.57	0.21	0.22	0.71	0.24	0.22	0.71	0.19	0.22	0.70
CSI	0.23	0.76	0.22	0.17	0.73	0.18	0.18	0.73	0.18	0.19	0.74	0.18

Table 4: Base rate (BR), frequency bias (FB), probability of detection (POD) or hit rate (HR), false alarm rate (FAR) mad critical success index (CSI) verification measures calculated for 24 hour accumulated precipitation and for ALADIN 2 km experiments (first row) for three categories (second row) for whole SOP1 period (5 September to 6 November 2012).

experiment	OPER			OSTIA			MUR			ROMS		
category	dry	medium	strong	dry	medium	strong	dry	medium	strong	dry	medium	strong
BR (%)	64.9	33.4	1.8	64.9	33.4	1.8	64.9	33.4	1.8	64.9	33.4	1.8
FB	0.96	1.07	1.28	0.96	1.07	1.21	0.96	1.07	1.18	0.96	1.07	1.15
POD/HR	0.87	0.79	0.37	0.88	0.79	0.34	0.88	0.80	0.34	0.87	0.80	0.33
FAR	0.09	0.26	0.71	0.09	0.26	0.72	0.09	0.25	0.71	0.09	0.26	0.72
CSI	0.80	0.62	0.19	0.81	0.62	0.18	0.81	0.63	0.18	0.81	0.63	0.18

Table 5: Base rate (BR), frequency bias (FB), probability of detection (POD) or hit rate (HR), false alarm rate (FAR) mad critical success index (CSI) verification measures calculated for 24 hour accumulated precipitation and for ALADIN 2 km experiments (first row) for three categories (second row) for whole SOP1 period (5 September to 6 November 2012) for IOP days.

experiment	OPER			OSTIA			MUR			ROMS		
category	dry	medium	strong	dry	medium	strong	dry	medium	strong	dry	medium	strong
BR (%)	18.1	74.8	7.1	18.1	74.8	7.1	18.1	74.8	7.1	18.1	74.8	7.1
FB	1.02	0.97	1.31	0.99	0.98	1.26	1.00	0.98	1.20	0.98	0.99	1.20
POD/HR	0.57	0.82	0.44	0.56	0.82	0.41	0.57	0.83	0.41	0.57	0.83	0.40
FAR	0.16	0.16	0.67	0.43	0.16	0.67	0.43	0.16	0.66	0.42	0.16	0.67
CSI	0.71	0.71	0.23	0.40	0.71	0.22	0.40	0.72	0.23	0.40	0.72	0.22

Table 6: Pierce's skill score (PSS) for 8 km and 2 km resolution forecasts.

model	HR88				HR22			
period	OPER	OSTIA	MUR	ROMS	OPER	OSTIA	MUR	ROMS
SOP1	0.68	0.64	0.64	0.64	0.67	0.67	0.68	0.68
IOP2	0.13	0.14	0.15	0.13	0.26	0.21	0.24	0.27
IOP4	0.17	0.19	0.17	0.17	0.26	0.24	0.25	0.23
IOP9	0.00	0.03	0.04	0.00	0.20	0.17	0.23	0.18
IOP12a	0.28	0.27	0.26	0.28	0.35	0.35	0.35	0.35
IOP13	0.24	0.17	0.20	0.24	0.51	0.53	0.53	0.51
IOP16c	0.16	0.17	0.14	0.16	0.33	0.33	0.31	0.30
IOP18	0.16	0.17	0.17	0.16	0.06	0.08	0.07	0.07
IOP19	0.06	0.07	0.06	0.06	0.60	0.60	0.59	0.58
IOPavg	0.19	0.18	0.18	0.19	0.40	0.40	0.41	0.40

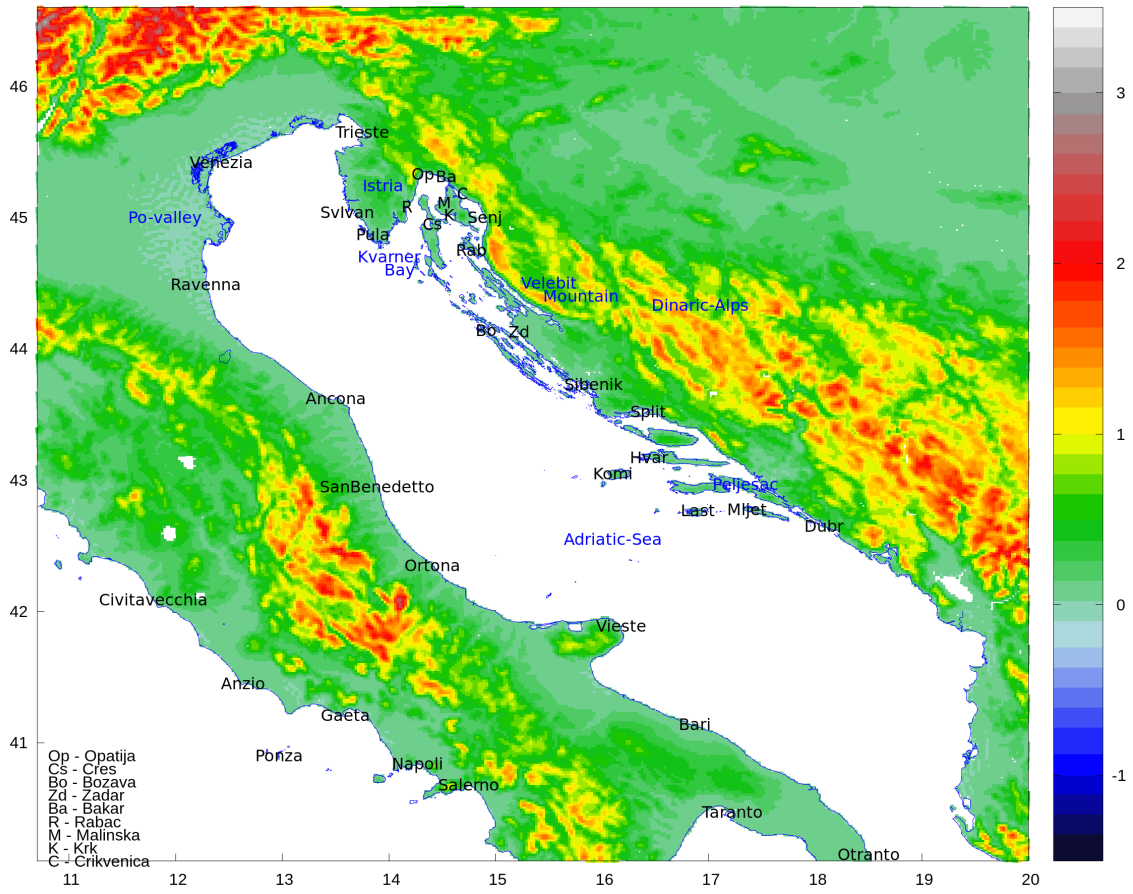

Figure 1: Map of Adriatic and Italian area with the locations of in situ SST measurements. The names of stations in Croatia are truncated due to large spatial density and explained in the lower left corner in the figure. The background is terrain height (in km) from 2 km resolution Aladin file, white means that land-sea mask is zero (sea or lake point in the model).

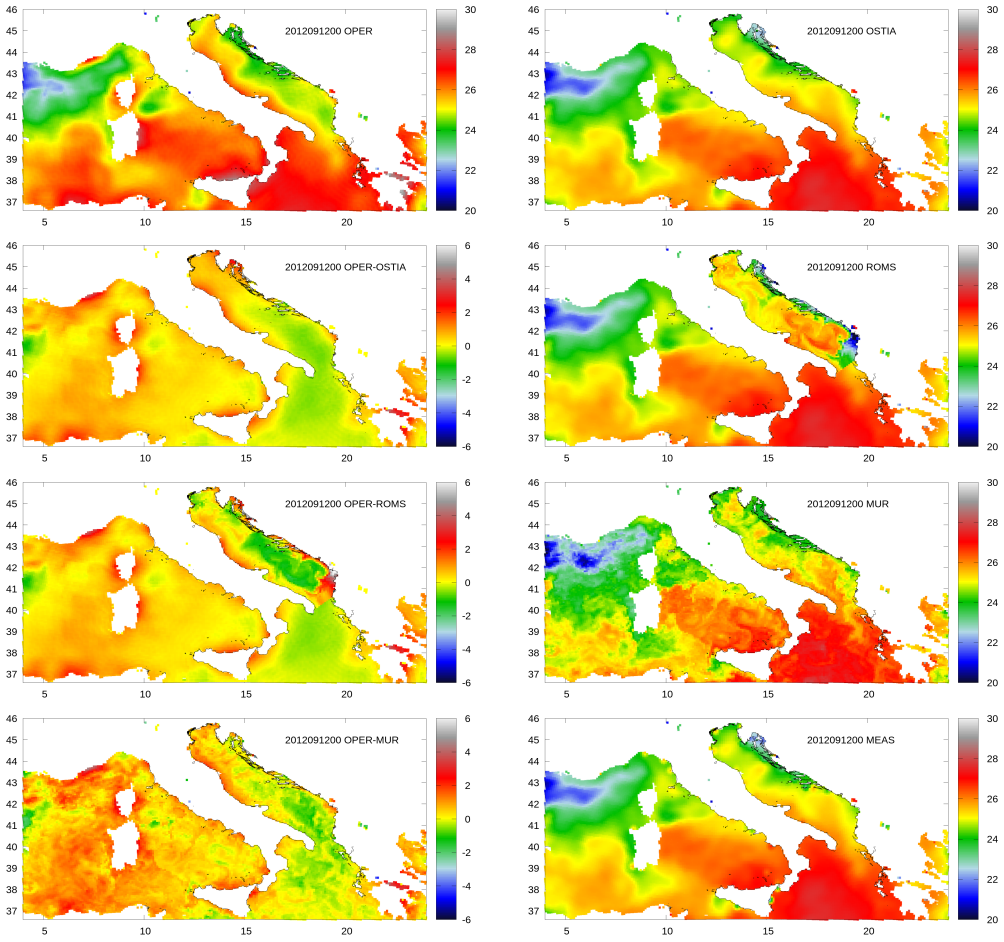

Figure 2: SST from the operational run in 8 km resolution (a), when OSTIA analysis is inserted (b), difference OPER-OSTIA (c), when ROMS is inserted in the field already modified by OSTIA (d), difference OPER-ROMS (e), when MUR analysis is inserted (f), difference OPER - MUR (g) and OSTIA inserted and nudged towards in situ measurements (h)for 00 UTC 12 September 2012.

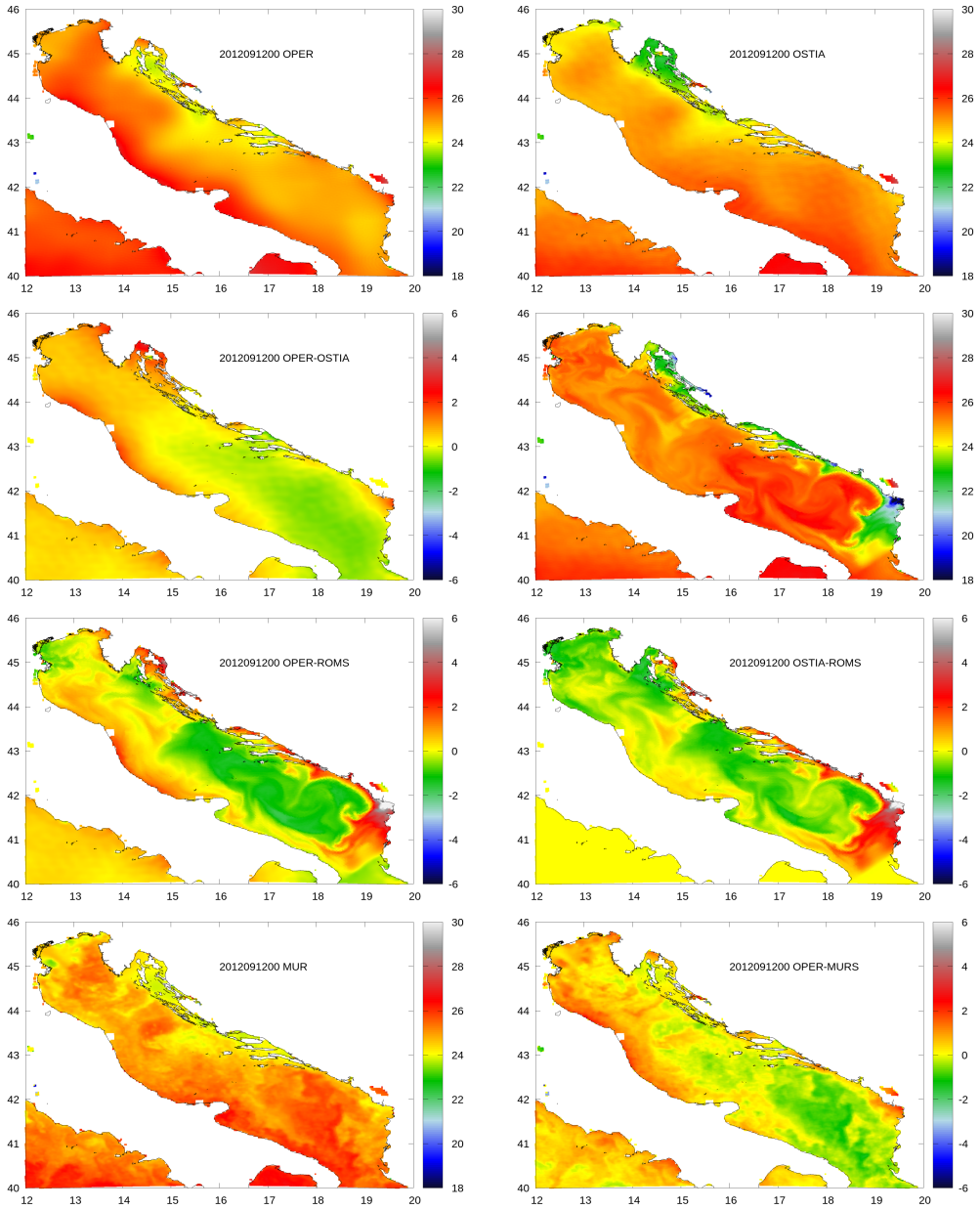

Figure 3: SST from the operational run in 2 km resolution (a), when OSTIA analysis is inserted (b), difference OPER-OSTIA (c), when ROMS is inserted in the field already modified by OSTIA (d), difference OPER-ROMS (e), and OSTIA-ROMS (f), when MUR analysis is inserted (g), difference OPER - MUR (h) for 00 UTC 10 September 2012.

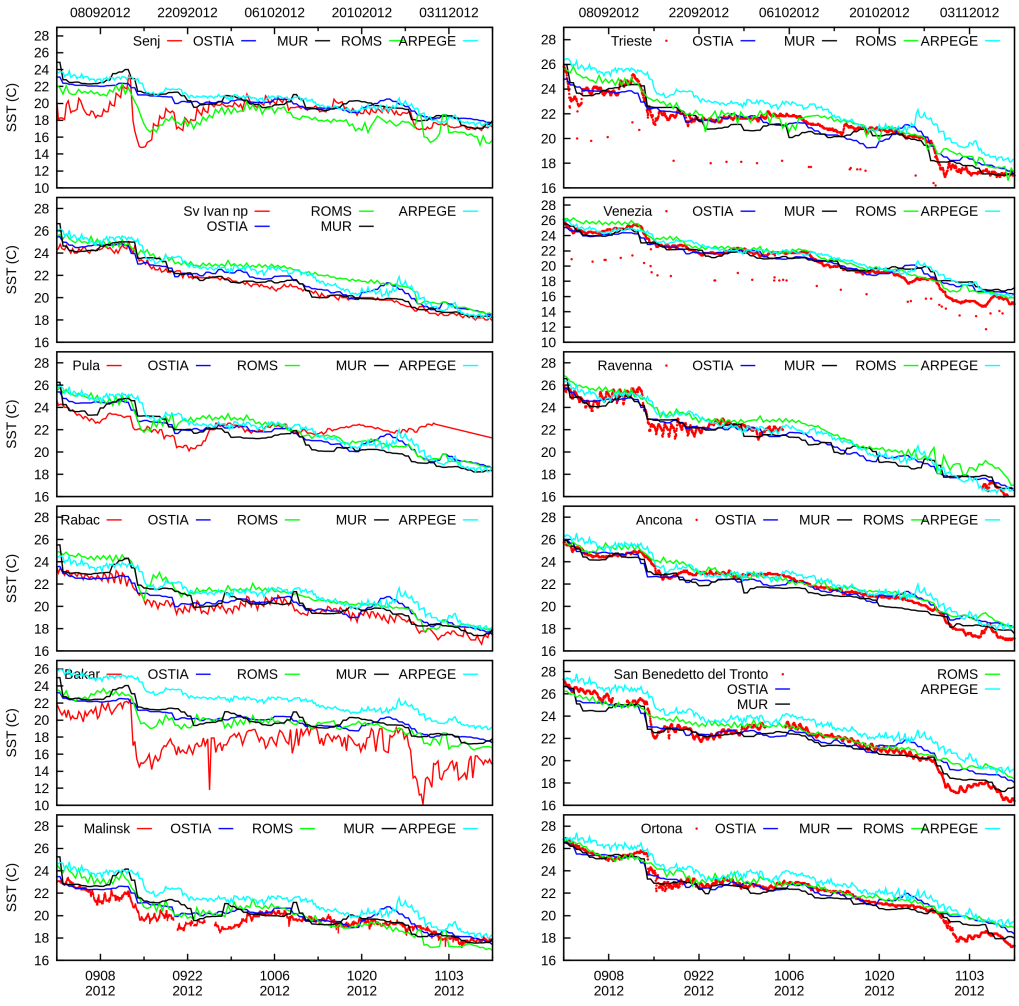

Figure 4: SST measured on station (red), from ARPEGE coupling files (cyan), OSTIA (blue), ROMS (green) and MUR (black) coupling files for different stations for the period from 1 September to 10 November 2012.

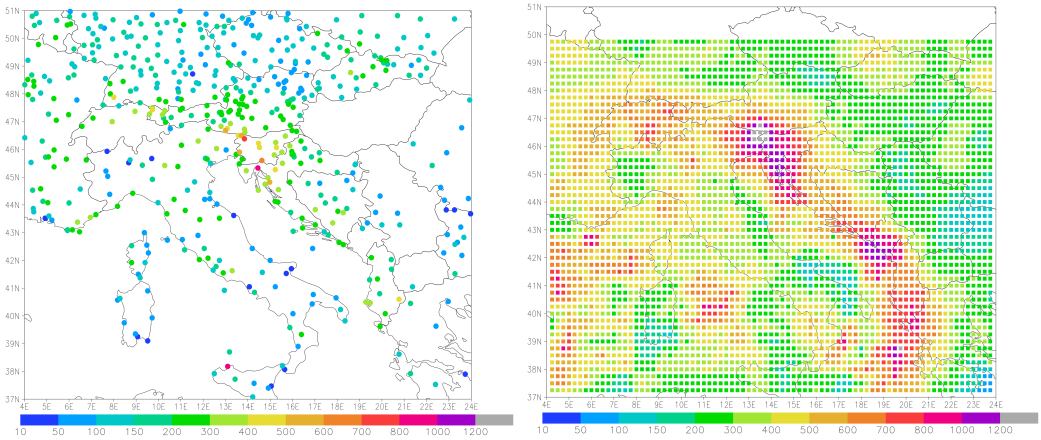

Figure 5: Precipitation (mm) accumulated during 61 days of SOP1 measured on SINOP stations (left) and TRMM estimate (right).

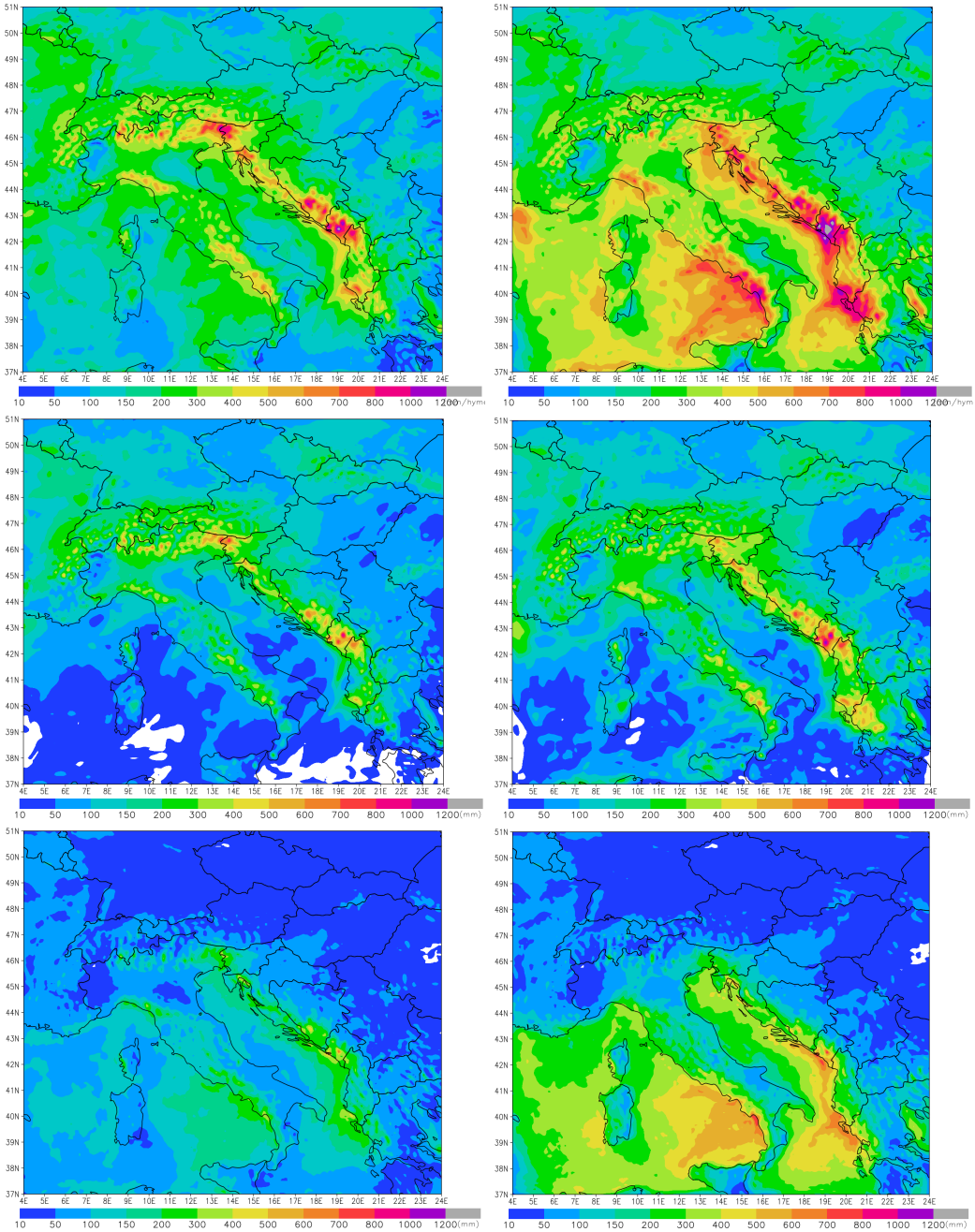

Figure 6: Precipitation (mm) accumulated during 61 days of SOP1 from 8 km resolution forecasts initiated at 00 UTC and accumulated from 06 to 30 hours of forecast: total (top row), resolved (middle row) and convective (bottom row) from operational forecast (left column) and experiment TM5K (right column).

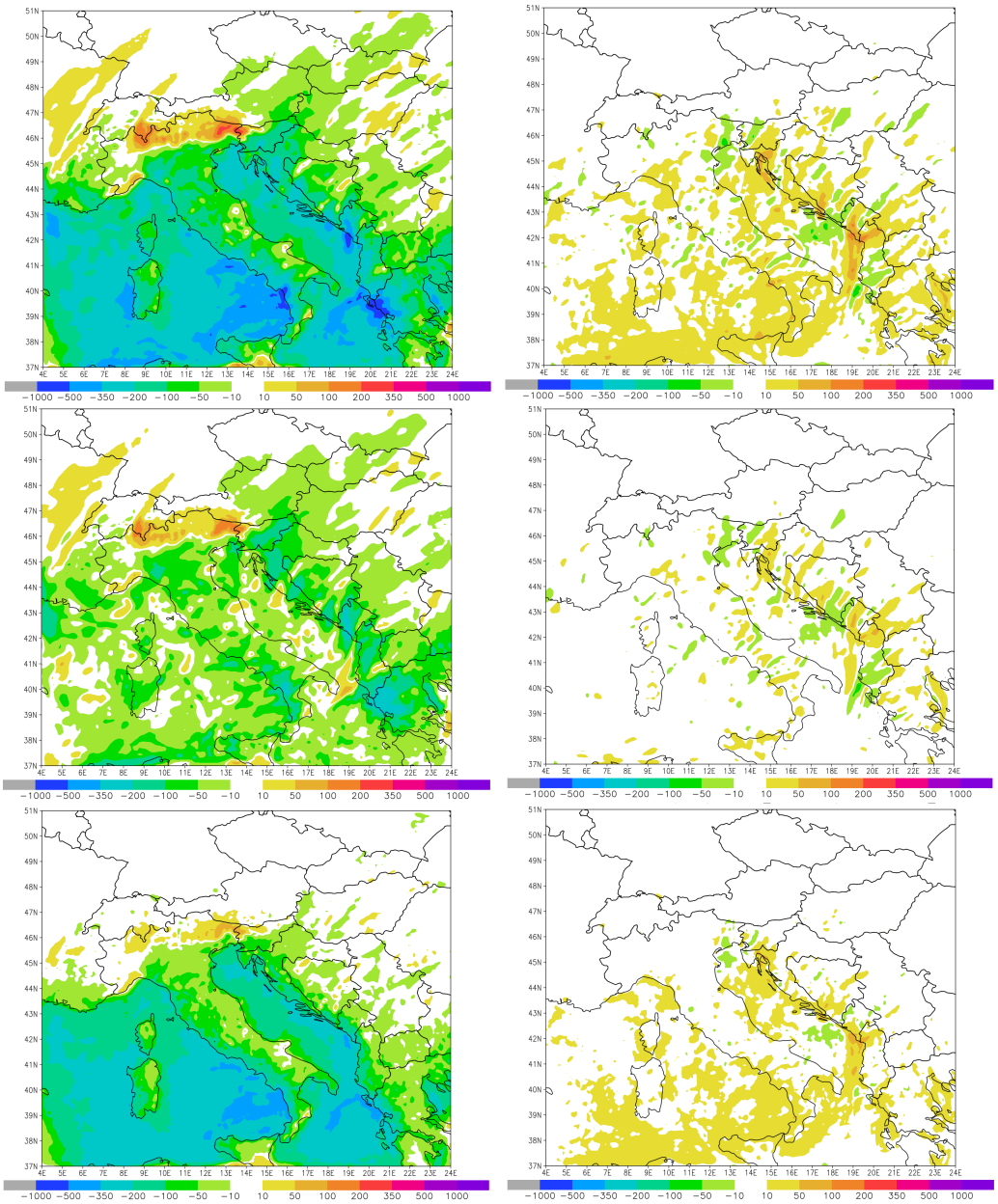

Figure 7: Precipitation difference (mm) accumulated during 61 days of SOP1 from 8 km resolution forecasts initiated at 00 UTC and accumulated from 06 to 30 hours of forecast: total (top row), resolved (middle row) and convective (bottom row) between the operational forecast and experiment TM5K (left colum) and between the operational forecast and experiment ROMS (right column).

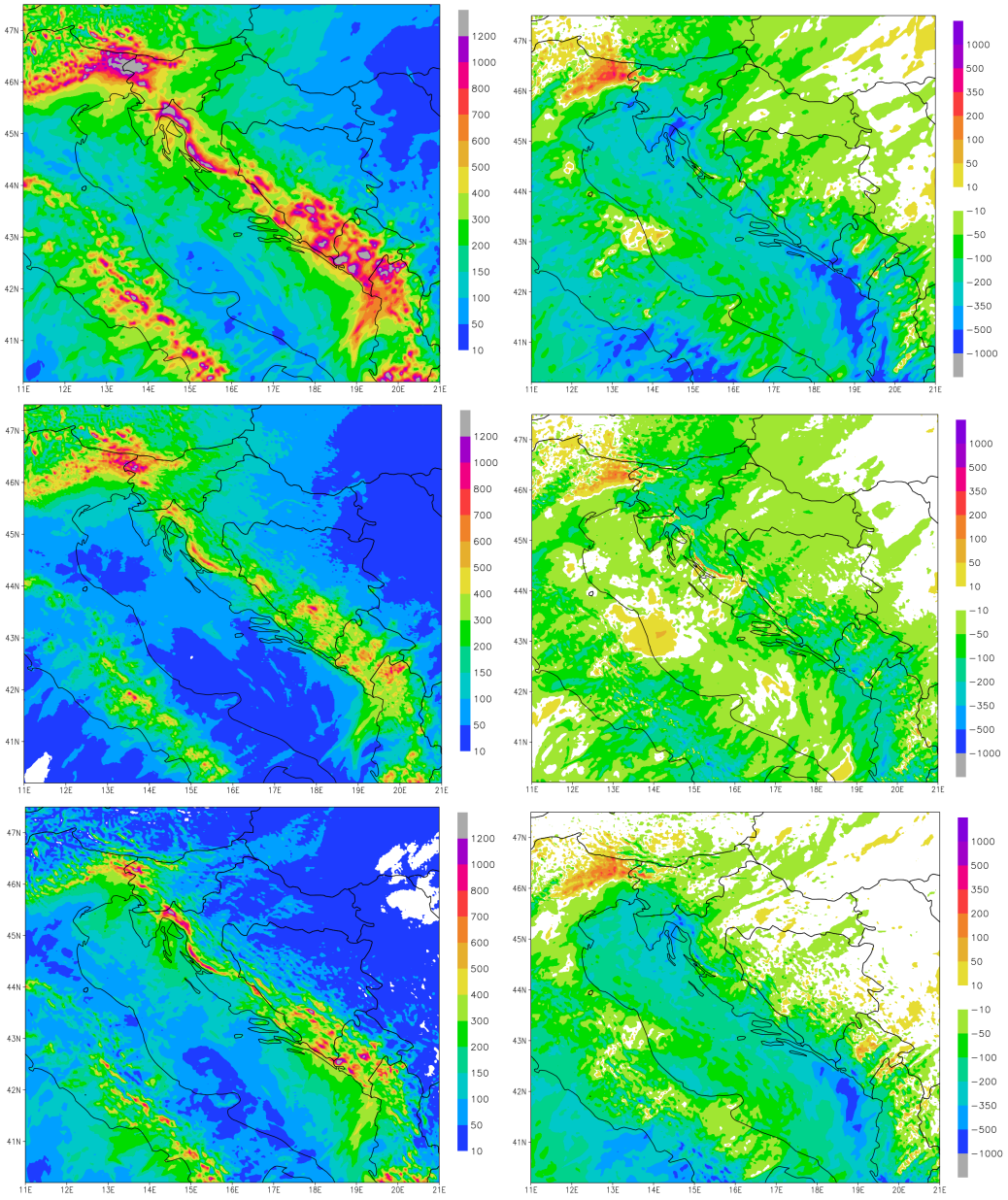

Figure 8: Precipitation (mm) accumulated during 61 days of SOP1 from 2 km resolution forecasts: total (top row), resolved (middle row) and convective (bottom row) from reference forecasts (left column) and difference between the TM5K and TP5K experiments (right column).

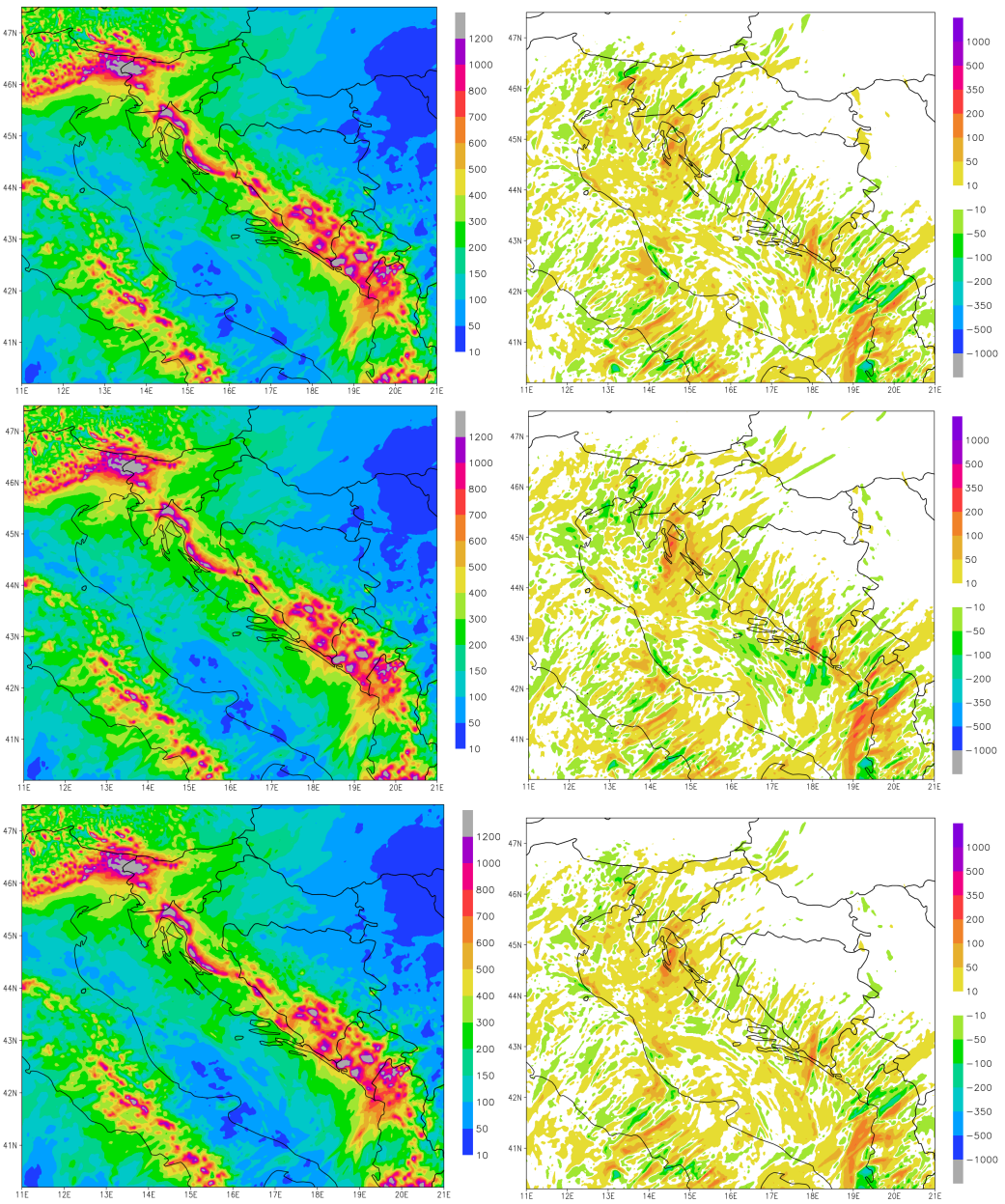

Figure 9: Precipitation (mm) accumulated during 61 days of SOP1 from 2 km resolution forecasts using SST from: OSTIA (top row), ROMS (middle row) and MUR (bottom row), accumulated values (left column) and difference to the reference (right column).

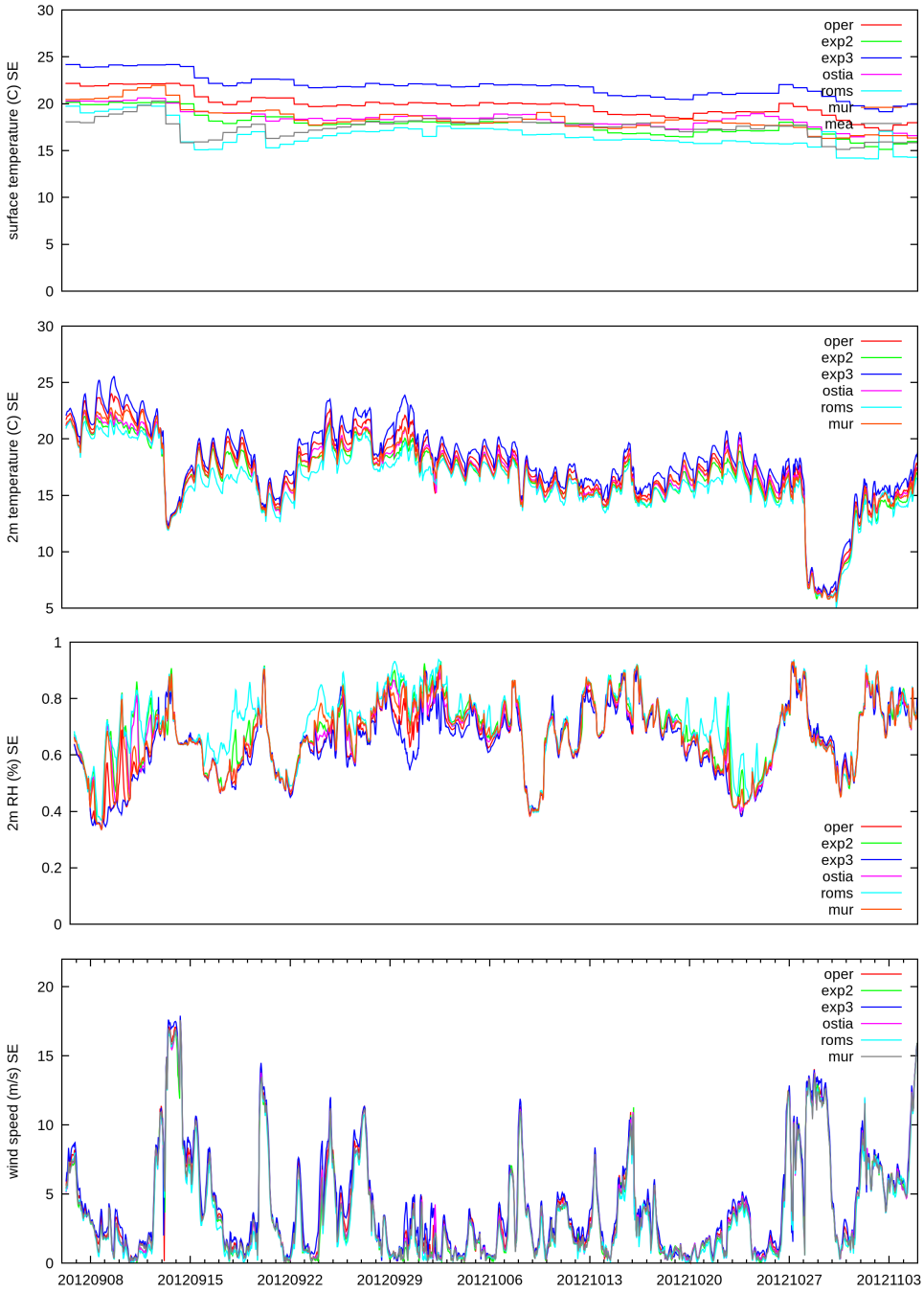

Figure 10: Surface temperature, 2 m temperature and relative humidity and wind speed from model forecasts in 2 km resolution during HyMeX SOP1. The values are averaged over a square with corners at longitude and latitude coordinates SW (14.7,44.7) NE (15.0,45.2) using only values over the sea points.

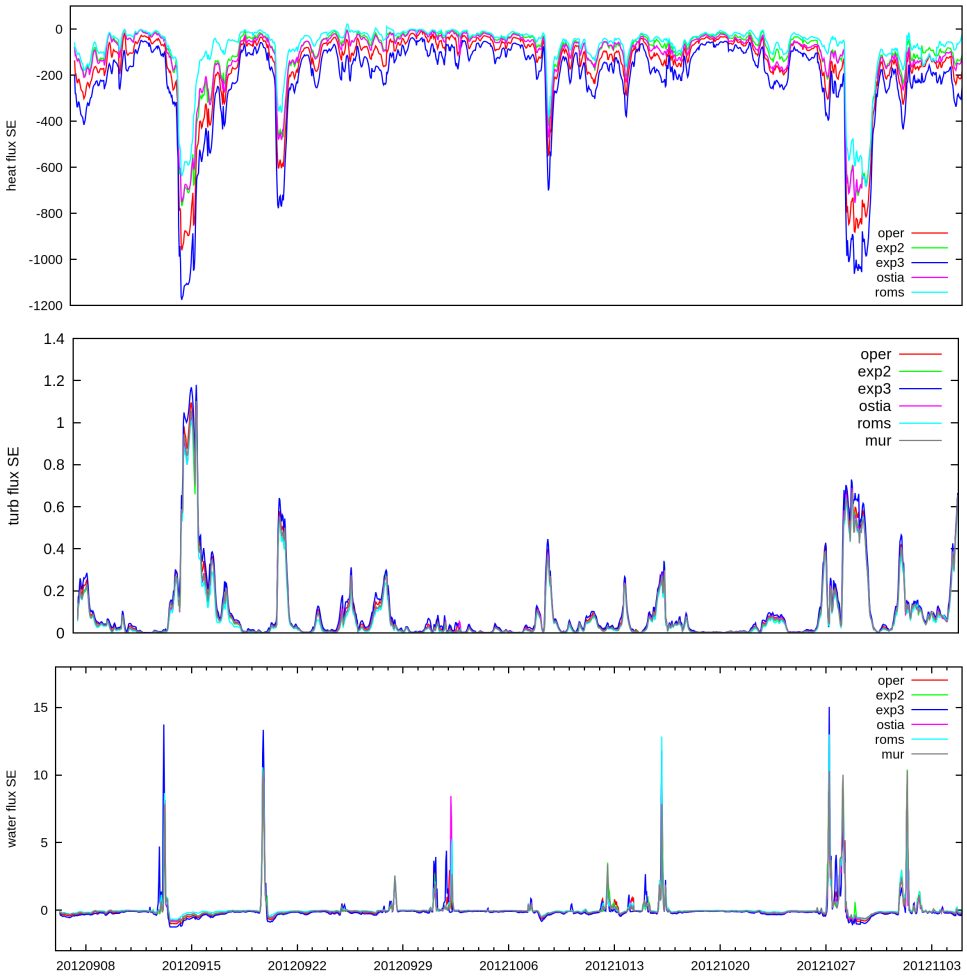

Figure 11: Total fluxes of heat (sensible+latent), turbulent flux of momentum and total water flux (precipitation + evaporation) from model forecasts in 2 km resolution during HyMeX SOP1. The values are averaged over a square with corners at longitude and latitude coordinates SW (14.7,44.7) NE (15.0,45.2) using only values over the sea points.

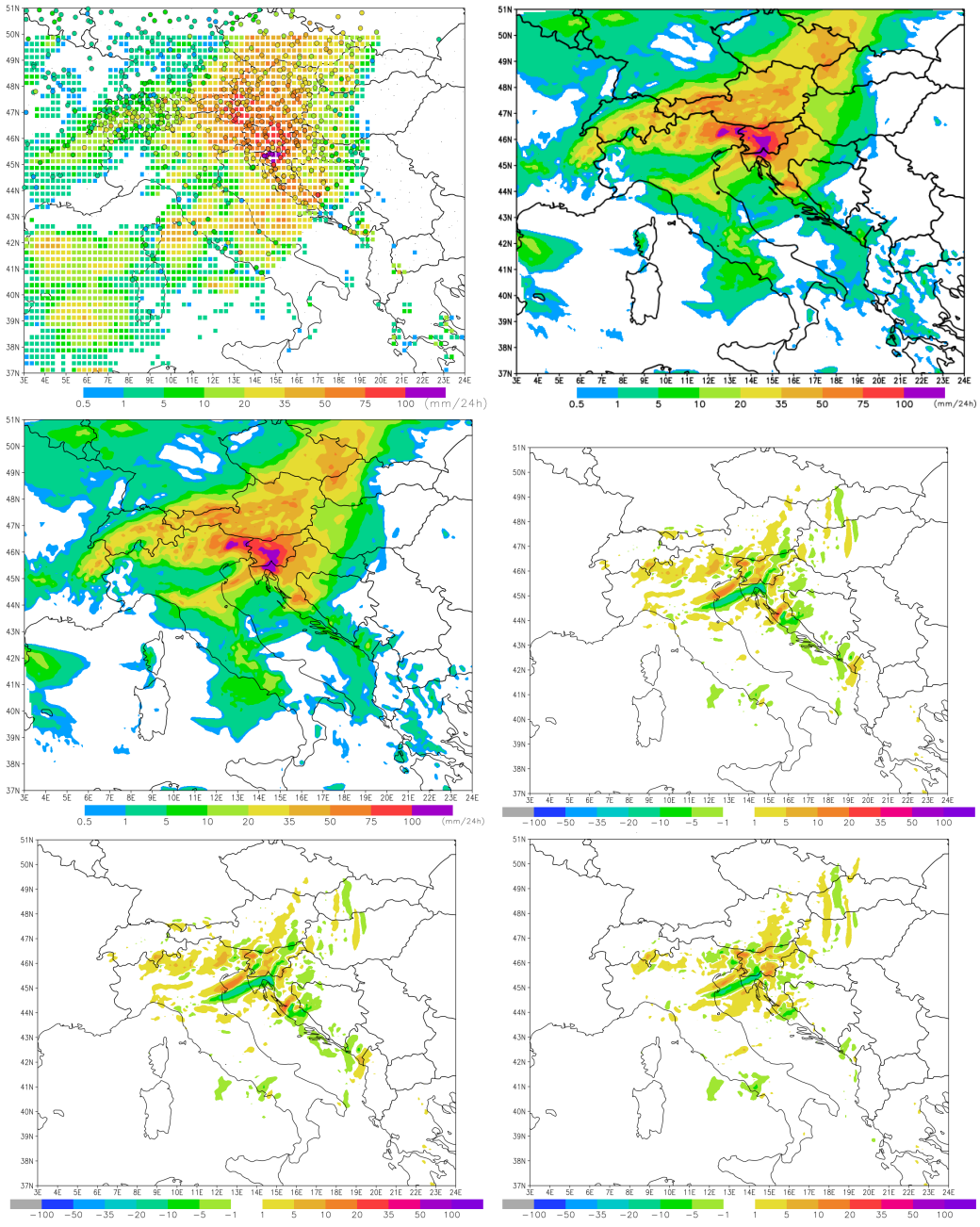

Figure 12: Accumulated 24 hourly precipitation starting from 06 UTC 12 September 2012, measured (top left) from rain gauges (circles) and TRMM estimate (squares), and forecasts: operational (top right), ROMS experiment (center left) and their difference (center right), the difference between OSTIA and ROMS experiments (bottom left) and between OPER and MUR experiments (bottom right) for the 8 km resolution domain, all runs starting from 00 UTC 11 September 2012.

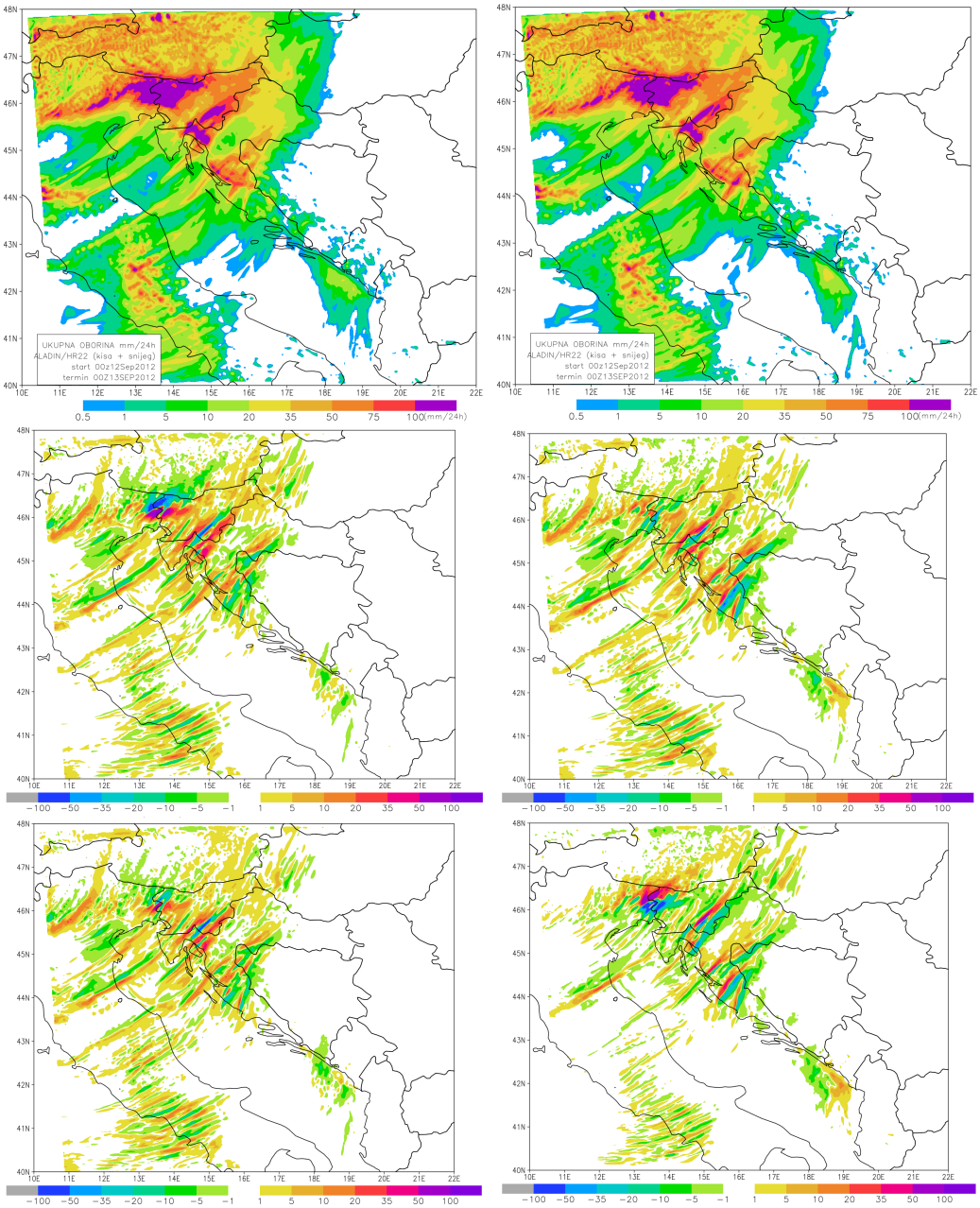

Figure 13: Accumulated 24 hourly precipitation starting from 06 UTC 12 September 2012 from 2 km resolution forecasts: reference (top left), ROMS experiment (top right), difference REF-OSTIA (center left), REF-ROMS (center right), REF-MUR (bottom left) and OSTIA-ROMS (bottom right).